1-1-2017

Engineering Of Organic Nanocrystals By Electrocrystallization

Mohamed Kilani
Wayne State University,

ENGINEERING OF ORGANIC NANOCRYSTALS BY ELECTROCRYSTALLIZATION

by

MOHAMED KILANI

THESIS

Submitted to the Graduate School

of Wayne State University,

Detroit, Michigan

in partial fulfilment of the requirements

for the degree of

MASTER OF SCIENCE

2017

MAJOR: MATERIALS SCIENCE & ENG.

Approved By:

_____

Advisor Date

DEDICATION

This work is dedicated to

my parents,

my sister,

my wife,

and my entire big family

for their unconditional love and support

ACKNOWLEDGMENT

I would like to express my deepest appreciation to the Fulbright program for offering me the opportunity to pursue my studies in Wayne State University. Besides the financial support, they gave me the chance to be part of a great community of talented and amazing people.

I would like to thank my adviser Dr. Guangzhao Mao for her guidance, supervision, and support during my master's. She opened the doors wide for me on a new area of research and pushed me to my limits through new challenges beyond the lab work.

Special thanks to Dr. Korosh Torabi for his teaching and fruitful discussions. The door to Dr. Torabi's office was always open whenever I had a question about my research.

I would like to thank Dr. Federico Rabuffetti for his suggestions for my research, and for accepting to be part of the evaluation committee.

Many thanks for my research group members, Xuecheng Yu, Fangchao Liu, Lingxiao Xie and all my friends, especially Deepak Joshi, Waleed Al-Ikhwan and Saad Al Bahlani and Ousama Elsaleh for their help and advice.

CONTENT

LIST OF TABLES

LIST OF FIGURES

I- Introduction:

Since Richard Feynman talk “there is plenty of room in the bottom” in 1959, until today, nanotechnology and nanoscience has been increasingly attractive for researchers and industrial companies, in many applications such as coating, textile, medicine, and electronics. One of the major applications is nanosensors. Thanks to their surface to volume ratio, the properties of the nanostructures are very sensitive to their environment. Many nanomaterials were employed in the gas sensing applications, where the major attention was given for the carbon nanotubes (CNT) and inorganic semiconductors such as ZnS or CdSe. These 1D nanomaterials exhibit ultra-high surface-to-volume ratio, sensitivity, selectivity, response, and low power consumption, and they offer a high commercial potential in a myriad of fields including industrial safety. The global gas sensor market is estimated to be about $20 billion, while the subset of the nanosensor segment is only $13.1 million in 2014. The small market size is partially attributed to the lack of feasible manufacturing techniques allowing utilization of many novel nanomaterials for sensor applications. The complexity and the cost have prevented rapid growth of domestic nanosensor market despite tremendous progress in nanomaterials research and nanotechnology.

Our research group discovered a solution-based, room-temperature crystallization process of making nanowires, which facilitates scalable manufacturing of nanowires directly on substrates and devices. The technique uses the electrocrystallization of organometallics and other charge-transfer compounds to produce conductive nanowires. The conductivity of these nanowires was shown to be sensitive to vapors like methanol, ammonia, and hydrogen sulfide. The technique could potentially solve some of the major problems of nanomanufacturing due to its simplicity, room temperature operation, and enabling the use of a wide range of new organic nanowires.

The shape and size control of the nanostructures is important because it determines the interfacial atomic arrangement of the material, thus it controls their properties. To date, majority of studies focus on using surfactants and surface-binding ligands to control the size of shape of nanoparticles synthesized in a solution. The interfacial energy between the crystal surfaces and the ligands determine the equilibrium shape of the crystal.

In this work, we show how to control the crystal morphology of organometallic materials with electrocrystallization and without using any additive ligands, relying only on the crystal properties. We show the thermodynamic/kinetic control by studying the effect of the electrochemical parameters on the crystal growth habit as well as the effect of the substrate nature. The material used for this work is the partially oxidized potassium tetracyanoplatinate ($K_{1.75}Pt(CN)_4 \cdot 1.5H_2O$) also known as Krogmann salt (K*(def)*TCP). The choice was made because of its anisotropic behavior and the high unidimensional conductivity.

Chapter 2 presents a literature review on the principles of nucleation and growth of crystals and their relationship with the electrochemical parameters. The various techniques for the crystal morphology control and the thermodynamic and kinetic control parameters are reviewed.

In chapter 3, the experimental methods used in the synthesis and characterization of the nanoparticles are described. The chapter covers the electrochemical setup as well as a brief presentation of the atomic force microscopy (AFM) and the scanning electron microscopy (FE-SEM).

In chapter 4, we show the results of the electrocrystallization of K(def)TCP. The effect of the concentration, the overpotential, and the current were studied. The results were evaluated and

analyzed, and a mathematical model that takes into consideration the different parameters is presented at the end of this chapter.

Chapter 5 covers the mathematical modeling and Monte Carlo simulations of the crystal growth behavior.

Chapter 6 summarizes the major conclusions of the work and makes a recommendation for future work.

II- Literature review

II-1- Basics of crystal formation

The interest of humans in crystals and crystallization extends back in history as far as the writings of men. The ancient peoples used crystals to make jewelries and for medical and religious purposes. Crystallization is used now for a myriad of applications and forms an important branch in modern science.

Crystallization can be defined as the formation of an organized solid phase from a liquid, gas, or a solution. When crystallized, the atoms or molecules assemble with a certain order, called the crystal structure, giving the solid its unique optical, electrical, and mechanical properties. The crystallization can occur naturally as in the formation of snowflakes or the geological formation of gemstones, or by industrial processes such as the cooling of melted solids and drug precipitation from a solution. Although the electrochemistry was discovered in 1796 by Alessandro Volta, the electrocrystallization was not used to control crystal formation until the beginning of the 20^{th} century. The electrical potential is used as a driving force to form the crystals. The electrocrystallization was primarily used for the electrodeposition of alloys and galvanic coatings, but it is widely used now for many applications. In this work, we use it to study and control the growth of nanoparticles and organic crystals.

The crystal formation involves two basic stages nucleation and crystal growth. We will review in this section the crystal formation mechanisms and the theoretical models that describe its thermodynamics and kinetics.

II-1-1- Nucleation

The nucleation is the first step in the crystal formation. The particles (atoms or molecules) accumulate together and create a cluster or a nucleus, when it reaches a certain size, the cluster grows and the crystal forms, otherwise it diminishes. When the particles assemble in the free space, it is called a homogeneous nucleation, however if it the nucleation happens on a foreign object, it is called a heterogeneous nucleation.

II-1-1-1- Classical nucleation theory

When the crystal is being formed, an energetic competition takes place between the surface and the internal volume. In the classical nucleation theory, the size of the nucleus r is a continuous variable and the change in the Gibbs free energy is written as the sum of the free energy of the created volume and the free energy of the created interface (Figure 1):

$$\Delta G = -\frac{4}{3}\pi r^3 \Delta\mu + 4\pi r^2 \gamma \qquad \text{Eq. 1}$$

Δμ is the new phase energy per unit volume or the driving force, and γ is the interfacial energy per unit area. The critical size r_c of the nucleus corresponds to the maximum of the change of the free energy $\left(\frac{\partial \Delta G}{\partial r}\Big|_{r_c} = 0\right)$. The crystal formation depends on the critical size and needs to overcome the energetic barrier:

$$r_c = \frac{2\gamma}{\Delta\mu} \qquad \text{Eq. 2} \qquad and \qquad \Delta G_c = \frac{16\pi}{3}\frac{\gamma^3}{\Delta\mu^2} \qquad \text{Eq. 3}$$

If the nucleus cannot overcome the energy barrier (ΔG_c) it dissolves, otherwise the crystal grows. The expressions show that both of the critical size and the energy barrier are

inversely proportional to the driving force $(\Delta\mu)$. This means that the nucleation is easier when the driving force is higher.

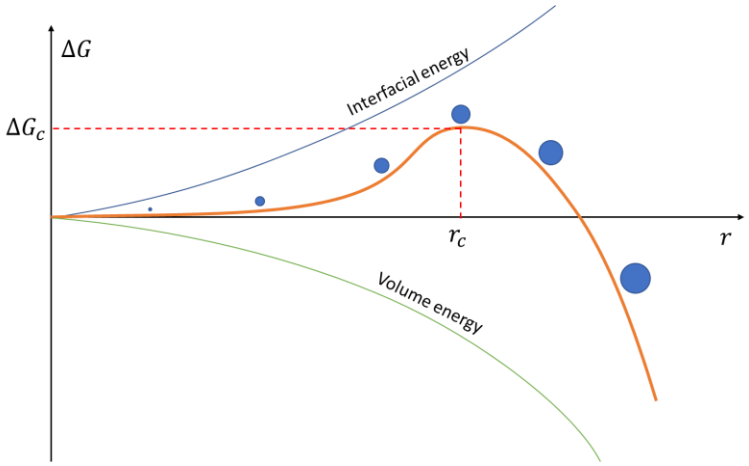

Figure 1- Evolution of the free energy with respect to the nucleus size

In the presence of impurities or foreign objects, the nucleation energy can change dramatically. The energy barrier reduces and the nucleation becomes relatively easier.

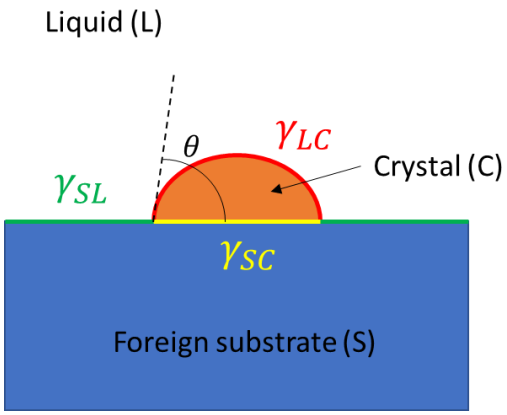

Figure 2- Heterogeneous nucleation

The change in the free energy can be expressed as follows:

$$\Delta G_{het} = -V\mu + S_{LC}\,\gamma_{LC} + S_{SC}\,\gamma_{SC} - S_{SC}\,\gamma_{SL} \qquad \text{Eq. 4}$$

The critical Gibbs free energy for the homogeneous nucleation is related to the one in homogeneous nucleation with a factor that depends on the angle θ:

$$\Delta G_{het} = f(\theta)\, \Delta G_{hom} \qquad \text{Eq. 5}$$

$$f(\theta) = \frac{(2 + cos\theta)(1 - cos\theta)^2}{4} \qquad \text{Eq. 6}$$

II-1-1-2- Atomistic nucleation theory

In the atomistic nucleation theory, the size of the nucleus is expressed with the number of particles that joined the crystal (Figure 3). The change in the Gibbs free energy is written as follows:

$$\Delta G = -n\Delta\mu + \Phi(n) \qquad \text{Eq. 7}$$

Δμ is the difference between the chemical potentials of the crystal and liquid phases, and Φ(n) is the interfacial energy. The critical size n_c of the nucleus corresponds to the maximum of the change of the free energy $\left(\frac{\partial \Delta G}{\partial n}\Big|_{n_c} = 0\right)$. The crystal formation depends on the critical size and needs to overcome the energetic barrier. This yields to the general condition for the crystal growth:

$$\Delta\mu = \frac{d\Phi(n)}{dn}\Big|_{n_c} \qquad \text{Eq. 8}$$

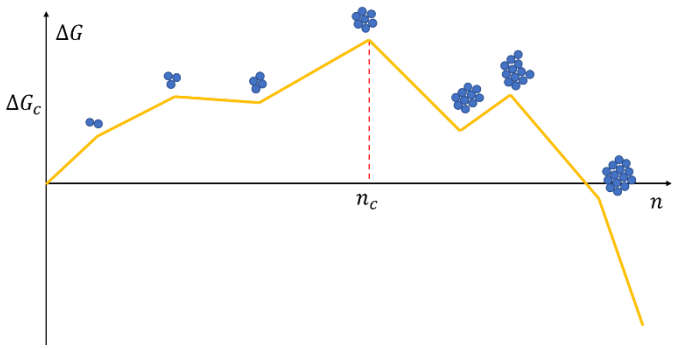

Figure 3- Evolution of the free energy with the atomistic approach

II-1-1-3- Nucleation rate

The rate of nucleation J(t) is the measure of how fast the transformation of the liquid particles into a nucleus of the new crystalline phase[1]. The steady state rate can be expressed using Arrhenius equation:

$$J = Z_0 W \lambda^{-1} exp\left(-\frac{\Delta G_c}{kT}\right) \qquad \text{Eq. 9}$$

Where Z_0 is the number density of active sites on the substrate, W is the frequency of attachment of particles to the nucleus and λ^{-1} is the Zeldovich factor which accounts for the difference between the quasi-equilibrium and the stationary number of critical nuclei. In the classical nucleation theory λ^{-1} has the following expression[1]:

$$\lambda^{-1} = \sqrt{\frac{\Delta G_c}{3\pi\, {n_c}^2\, kT}} \qquad \text{Eq. 10}$$

II-1-2- Crystal growth

Crystal growth is the step after the formation of a stable nucleus. It consists of series of processes by which particles attach to the surface of the crystal allowing the expansion of the crystal size. The crystal growth process can be summarized as follows[1]:

1- Diffusion of particles in the solution

2- Adsorption/attachment the particles to the surface

3- Hopping of particles on the surface

4- Attachment of particles to edges

The first process happens in the solution before being attached to the crystal, the three last ones happen on the surface. The processes occur in series, so the overall rate is governed by the slowest one. The overall crystal growth is transport controlled if the first step is the slowest, however it is surface controlled if the surface steps are slower.

The surface energies and kinetics define the crystal shape and size. We will discuss how to control the crystal morphology using thermodynamics and kinetics in the paragraph II-2.

II-1-3- Thermodynamics of the crystal growth

The change in the free energy of the system {crystal, substrate, solution} can be written as:

$$dG = -SdT + VdP - \mu_L dN_L + \mu_C dN_C + \sum_i \gamma_i \, dS_i \qquad \text{Eq. 11}$$

At constant temperature and pressure, and when the net rate of particles exchange between the crystalline and the solution phases is zero, the free energy is:

$$dG = \sum_i \gamma_i \, dS_i \qquad \text{Eq. 12}$$

At equilibrium, the free energy is minimized and the crystal volume is constant ($\delta V = \delta(\sum h_i S_i) = 0$):

$$dG = \sum_i \gamma_i \, dS_i = 0 \qquad \text{Eq. 13}$$

$$\sum_i S_i \, \delta h_i = \sum_i h_i \, \delta S_i = 0 \qquad \text{Eq. 14}$$

The combination of both conditions gives the Wulff theorem:

$$\frac{\gamma_1}{h_1} = \frac{\gamma_2}{h_2} = \cdots = \frac{\gamma_n}{h_n} \qquad \text{Eq. 15}$$

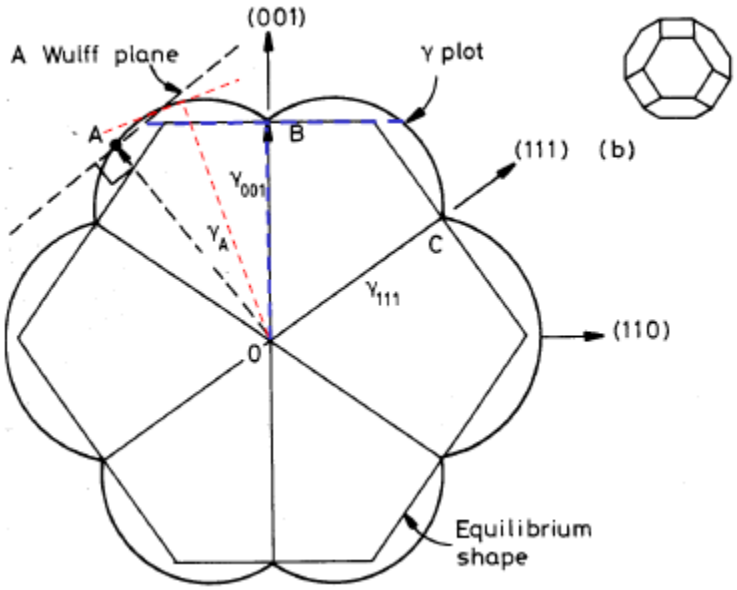

Figure 4- Illustration of the Wulff construction

γ_1, γ_2… γ_n are the surface energies of the different facets of the crystal. In solids, the surface energy is defined as the necessary free energy to create the new surface. The creation of new surfaces needs the rupture of some atomic bonds across the surface. For covalently bonded crystals, only bonds between nearest neighbors are considered (Harkin's model). The surface energy of a crystallographic plane can be calculated as follows:

$$\gamma = \frac{\frac{number\ of\ broken\ bonds}{surface\ atom} \times bond\ energy}{2 \times area\ per\ atom}$$

In order to include the interaction with further layers, Harkin's model can lead to some errors, especially for high crystallographic indices. Density functional theory (DFT) calculations offers a more accurate method to calculate the interfacial energies

The Wulff theorem suggests that in equilibrium, the interfacial energies of the crystal facets are the only factor that determines the crystal shape: the relative growth rate of the facets is equal to the surface energy ratio $\left(\frac{\dot{h}_i}{\dot{h}_j} = \frac{\gamma_i}{\gamma_j}\right)$. Despite the beauty of the theorem, the experiments showed that the thermodynamics is not sufficient to define the crystal shape, and the kinetic parameters of the crystal growth have an effect on the morphology as described in the following section.

II-1-4- Kinetics of the crystal growth

The kinetics of the different growth steps govern the overall kinetics of the crystal growth. The first step for the molecules to be attached to the crystal is to travel from the solution to the crystal surface. The driving force of the molecular diffusion is the solution concentration gradient. When the first particles create the critical nucleus, the surrounding particles will join the crystal, which will create a layer of a dilute zone around the crystal. That will push the particles in the rest of the solution to move and restore the homogeneous concentration. The diffusion phenomenon was studied by Adolf Fick in 1855 who modeled it with two laws[2]:

$$\overrightarrow{J(r,t)} = -D\ \vec{\nabla} C(r,t) \qquad \text{Eq. 16}$$

$$\frac{dC(r,t)}{dt} = D\ \Delta C(r,t) \qquad \text{Eq. 17}$$

Where $C(r,t)$ is the concentration of the solution, $\overrightarrow{J(r,t)}$ is the diffusion rate, D is the diffusion constant, $\vec{\nabla}$ is the gradient operator and Δ is the Laplacian operator.

The first law (15) describes how the diffusion rate is related to the gradient of the concentration: the particles travel from the zones of high concentration to lower concentration. The second law describes how the concentration changes over time function of the spatial distribution of the concentration.

The kinetics of the surface attachment follow the general rules of chemical reactions. The particles need to overcome an energy barrier to join the crystal, and the rate is proportional to the concentration of the solution:

$$R = kC^{\alpha}e^{-\frac{\Delta G}{kT}} \qquad \text{Eq. 18}$$

α is the order of the reaction and k is a proportionality constant. The rate of surface attachment can be controlled by changing the concentration, the temperature, or an external potential.

In electrocrystallization, the growth rate can be controlled with the applied potential. We will discuss the thermodynamic and kinetic mechanisms of the electrocrystallization in the next section.

II-2- Mechanisms of electrocrystallization

The electrocrystallization is a crystallization reaction where the driving force is the electric potential. It is a first order phase transition occurring at electrochemical solid/liquid interfaces. We will discuss in this section the concepts of the electrochemical setup, the thermodynamics and the kinetics of the electrocrystallization reaction.

II-2-1- Electrochemical setup

An electrochemical reaction is a redox reaction which involves electron transfer at the interface between an electrode and an electrolytic solution. If a chemical reaction can generate spontaneously an electric current when the electrodes are connected with a conductor, in this case we obtain a galvanic cell. An electrolysis however uses an external electric potential to produce a chemical reaction. The reaction takes place in an electrolytic cell.

The electrolytic cell is composed of an electrolytic solution which contains the electroactive species, the electrodes where the application of the electric potential and transport the current occur, and a potentiostat/galvanostat that controls and measures the electric parameters.

Many configurations can be used to make an electrolytic cell. The most common systems are two-electrodes, three-electrodes, and four electrodes. The most basic one is the two-electrode setup, where we apply an electric potential between the working electrode (WE) and the reference electrode (RE). Despite its simplicity, this system has a measurement issue because the potential and the current cannot be measured separately. The three-electrode system fixes the problem by adding the counter electrode (CE) to separate the current from the potential references. There is also a four-electrode system, not very common, usually used in impedance measurement of the electrolytic solution. In this work, we use only the three-electrode system.

In the three-electrode system (Figure 5), the working electrode (WE) is where the reaction of interest is happening (electrocrystallization in our case), and it is usually made of an inert material, such as gold or platinum to form a foreign substrate for the heterogeneous nucleation. The reference electrode (RE) has a fixed potential that serves as a reference for the control and the measurement of the electrolytic cell potential. The current flow through RE is

zero because of its high impedance. The counter electrode (CE) is the one that closes the electric circuit and make the current flow possible. It is also made of an inert material and do not participate in the reaction.

All the three electrodes are connected to a potentiostat or a galvanostat which are electronic instruments that control and measure the electric parameters (potentials and currents) of the electrochemical cell (Figure 6). While they have the same basic electronic configuration, the potentiostat controls the potential difference between WE and RE so that it is equal to the value specified by the user (Einput). The galvanostat, in the other hand, controls the current flow between CE and WE. The user can switch between the two modes (by switching the position of S).

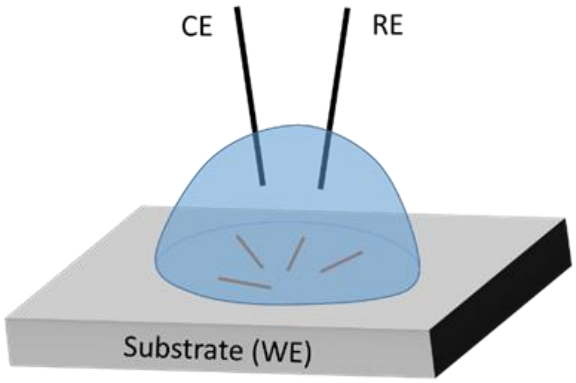

Figure 5- Three-electrode electrochemical setup

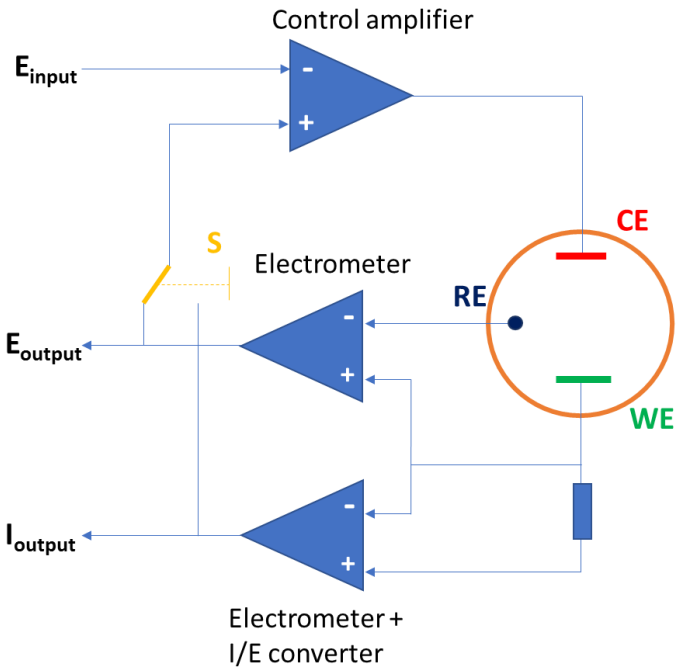

Figure 6- Simplified scheme of a potentiostat/galvanostat

II-2-2- Thermodynamics of electrocrystallization

Gibbs was the first to study the electrocrystallization theoretically in 1899. He introduced the electrochemical potential of the different phases of the system to make the relationship between the chemical and the electric potential[1–3]:

$$\tilde{\mu} = \mu^0 + kT\ln(a) + ze\phi \qquad \text{Eq. 19}$$

$\mu^0$is the standard chemical potential, k is Boltzmann constant, T is the temperature, a is the activity, z is the valence of the material ions, e the electron charge, and ϕ is the electric potential.

An electrochemical system is composed of an electrolyte solution of the material ions (M^z), where z is the valence and $\tilde{\mu}_{s,eq}$is its electrochemical potential, a crystal of the same material (M) where $\tilde{\mu}_{c,eq}$is its electrochemical potential and $\phi_{we,eq}$is its Galvani potential, and an

inert foreign substrate as a working electrode whose Galvani potential is $\phi_{we,eq}$. When adsorbed in the foreign substrate the particles will have the electrochemical potential $\tilde{\mu}_{ad,eq}$. At the equilibrium state, all the electrochemical potentials are equal, and we get the following equation:

$$\tilde{\mu}_{s,eq} = \tilde{\mu}_{c,eq} = \tilde{\mu}_{ad,eq} \qquad \text{Eq. } 20$$

Where:

$$\tilde{\mu}_{s,eq} = {\mu_s}^0 + kT\ln\left(a_{s,eq}\right) + ze\phi_{s,eq} \qquad \text{Eq. } 21$$

$$\tilde{\mu}_{c,eq} = {\mu_c}^0 + ze\phi_{c,eq} \qquad \text{Eq. } 22$$

$$\tilde{\mu}_{ad,eq} = {\mu_{ad}}^0 + kT\ln\left(a_{ad,eq}\right) + ze\phi_{c,eq} \qquad \text{Eq. } 23$$

The combination of equations 11, 12 and 13 leads to Nernst equation:

$$E_{eq} = E^0 + \frac{kT}{ze}\ln\left(a_{s,eq}\right) \qquad \text{Eq. } 24$$

Where $E_{eq} = \phi_{c,eq} - \phi_{s,eq}$is the equilibrium potential and $E^0 = \frac{\left({\mu_s}^0 - {\mu_c}^0\right)}{ze}$ is the standard potential. Nernst equation describes the electrochemical relations between the electric and chemical potential in equilibrium state.

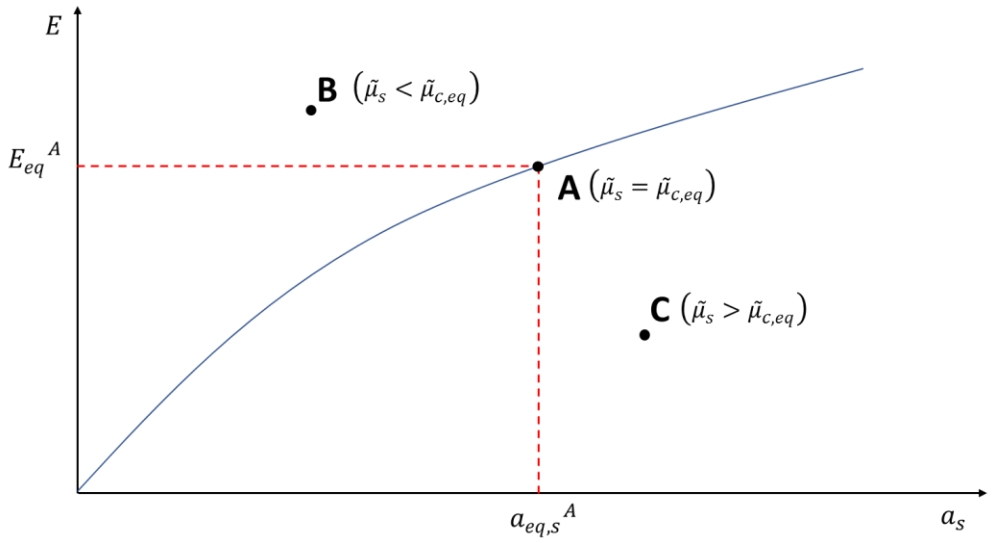

Figure 7- Equilibrium diagram for a crystal with its ionic solution

When the system deviates from the equilibrium, it can be in one of two states: if the electrochemical potential of the crystalline phase $\tilde{\mu}_{c,eq}$ is lower than the electrochemical potential of the solution $\tilde{\mu}_s$ we get the electrochemical supersaturation (point C in figure-4), else when $(\tilde{\mu}_s < \tilde{\mu}_{c,eq})$ we get the electrochemical undersaturation. The electrochemical system tends always to go to the equilibrium $(\tilde{\mu}_s = \tilde{\mu}_{c,eq})$, so if it is in the supersaturation state the particles will transform from the ionic solution to the crystalline phase, which results in the crystal formation and growth. Contrariwise, when the system is undersaturated, the crystalline phase will dissolve into the solution.

The state of the system can be defined by evaluating the quantity $\Delta\tilde{\mu} = \tilde{\mu}_s - \tilde{\mu}_{c,eq}$. $\Delta\tilde{\mu}$ is the driving force of the electrochemical phase transition. It can be expressed function of the controllable physical quantities (electrical and chemical):

$$\Delta\tilde{\mu} = ze\eta \qquad \text{Eq. 25}$$

Where:

$$\eta = E_{eq} - E \qquad \text{Eq. 26} \quad \text{or}$$

$$\eta = \frac{kT}{ze}\ln\left(\frac{a_s}{a_{s,eq}}\right) \qquad \text{Eq. 27}$$

η is called the cathodic overpotential. It is clear from the equations 17 and 18 that the supersaturation/undersaturation can be controlled either by manipulating the electric potentials (E, E_{eq}) or the chemical activities (a_s, $a_{s,eq}$).

II-2-3- Kinetics of electrocrystallization

The kinetics of electrocrystallization are the same kinetics of the nucleation and crystal growth in heterogeneous crystallization, but with a specific driving force which is the electric potential. The nucleation rate has the same expression as Eq. 9, where the frequency of attachment is[1]:

$$W = k_v \exp\left(-\frac{U}{kT}\right)\exp\left(-\frac{\alpha zeE}{kT}\right) \qquad \text{Eq. 28}$$

$k_v$is a proportionality factor, α is the charge transfer coefficient and U is the energy barrier to transfer an ion from the electrolyte to the critical nucleus at an electric potential E=0. The stationary nucleation rate J_0 at $\lambda^{-1} \rightarrow 1$ is[1]:

$$J_0 = Z_0 k_v \left(\gamma_{eq} C_{eq}\right)^{1-\alpha} \exp\left(-\frac{U + \alpha zeE^0 + \Phi(n_c)}{kT}\right)\exp\left(\frac{(n_c + \alpha)ze\eta}{kT}\right) \qquad \text{Eq. 29}$$

Where $C_{eq}$is the equilibrium concentration of the electrolytic solution and γ_{eq} is the corresponding activity coefficient ($a_{eq} = C_{eq}\gamma_{eq}$).

The rate of the crystal growth obeys the kinetics law of a first order reaction:

$$R = kC(0,t)\exp\left(-\frac{\Delta G}{kT}\right) \qquad \text{Eq. 30}$$

$C(0,t)$ is the concentration at the interface of the electrode. The net rate is the difference between the rates of the reduction and oxidation reactions:

$$R_{net} = k_O C_O(0,t)\exp\left(-\frac{\Delta G_O}{kT}\right) - k_R C_R(0,t)\exp\left(-\frac{\Delta G_R}{kT}\right) \qquad \text{Eq. 31}$$

Leading to the current-potential relationship known as Butler-Volmer formulation[2]:

$$i = zeAk_0\left(C_O(0,t)\exp\left(-\frac{\alpha ze(E-E^0)}{kT}\right) - C_R(0,t)\exp\left(\frac{(1-\alpha)ze(E-E^0)}{kT}\right)\right) \qquad \text{Eq. 32}$$

The net current of the electrocrystallization reaction is proportional to the rate. By including the bulk concentrations, we can establish a current-overpotential relationship[2]:

$$i = i_0\left(\frac{C_O(0,t)}{C_{Ob}}e^{-\frac{\alpha ze\eta}{kT}} - \frac{C_R(0,t)}{C_{Rb}}e^{\frac{(1-\alpha)ze\eta}{kT}}\right) \qquad \text{Eq. 33}$$

$i_0 = zeAk_0{C_{Ob}}^{(1-\alpha)}{C_{Rb}}^{\alpha}$ is the exchange current, C_{Ob} and C_{Rb} are the bulk concentrations, and $\eta = E - E_{eq}$ is the overpotential. The Butler-Volmer equation is a fundamental relationship between the current, the potential and the concentration of the electrolytic cell. The first part counts for the anodic current, while the second is the cathodic current (Figure 8).

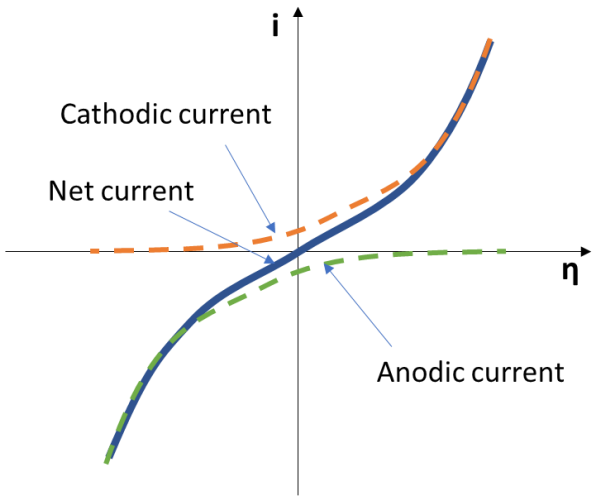

Figure 8- The cathodic, anodic, and net current density as function of the overpotential

II-3- Synthesis of cation-deficient potassium tetracyanoplatinate K*(def)*TCP

II-3-1- Krogramann's salts

Krogmann's salts were discovered by the German Klaus Krogmann in 1960. They are characterized by a chain of square planar coordination complex of platinum and cyanide. The platinum chain gives the compounds unique electric properties that make them very interesting for many applications. One of the interesting chemical properties of these compounds is the possibility to partially oxidize the tetracyanoplatinate groups containing platinum atoms in a nonintegral oxidation state. This property enables the production of a wide variety of new chemical products with different optical and electric properties.

The modification of the chemical composition of Krogmann's salts can change the interatomic distance between platinum in the tetracyanoplatinate chain (Table 1). The Pt-Pt distance variation can produce a variety of compounds from electric insulators to materials with one dimensional metallic conductivity. This property is the result of the overlapping of the Pt dz2

orbitals which creates electron delocalization (Figure 9). The electrical conductivity along the platinum chain can be 10^5 greater than the conductivity perpendicular to the chain.

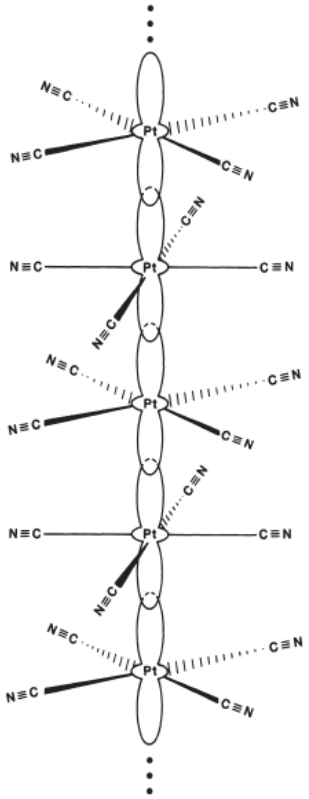

Figure 9- Chain of $[Pt(CN)_4]$ showing the overlapping of Pt d_z^2 orbitals[4]

Table 1- Crystal Structure and Conductivity of Partially Oxidized Tetracyanoplatinate Metals[4]

Complex	Abbreviation	Space group[a]	Intrachain separation d_{Pt-Pt} (Å) ($T = 298$ K)	Conductivity (Ω^{-1} cm^{-1})[b]	Color
Pt metal			2.775[66]	9.4×10^4	Metallic
$K_2[Pt(CN)_4]Br_{0.30} \cdot 3H_2O$	KCP(Br)	$P4mm$[a,c]	2.89	4–1050	Bronze[86]
$K_2[Pt(CN)_4]Cl_{0.30} \cdot 3H_2O$	KCP(Cl)	$P4mm$[68]	2.87	~ 200	Bronze[86]
$K_2[Pt(CN)_4]Br_{0.15}Cl_{0.15} \cdot 3H_2O$	KCP(Br, Cl)	$P4mm$[69]		—	
$Rb_2[Pt(CN)_4]Cl_{0.3} \cdot 3H_2O$	RbCP(Cl)	$P4mm$[70,71]	2.877(8) and 2.924(8) at $T = 298$ K[70]; 2.885(6) and 2.862(6) at $T = 110$ K[71]	10^{90}	Bronze
$Cs_2[Pt(CN)_4]Cl_{0.3}$	CsCP(Cl)	$I4/mcm$[72]	2.859(2)	~ 200[93]	Bronze
$(NH_4)_2(H_3O)_{0.17}[Pt(CN)_4]Cl_{0.42} \cdot 2.83H_2O$	ACP(Cl)	$P4mm$[73]	2.910(5) and 2.930(5)	0.4[92]	Bronze
$Cs_2[Pt(CN)_4](N_3)_{0.25} \cdot 0.5H_2O$	CsCP(N_3)	$P\bar{4}b2$[74]	2.877(1)	—[d]	Reddish-copper
$Rb_3(H_3O)_x[Pt(CN)_4](O_3SO \cdot H \cdot OSO_3)_{0.49} \cdot (1-x)H_2O$	RbCP(DSH)	$P\bar{1}$[75]	2.826(1)	—[d]	Copper

$K_{1.75}[Pt(CN)_4]\cdot 1.5H_2O$	K(def)TCP	$P\bar{1}$[76]	2.965(1) and 2.961(1)	115–125[95,96,105]	Bronze
$Rb_{1.75}[Pt(CN)_4]\cdot xH_2O$	Rb(def)TCP	—[e,77]	2.94[100]	1[105]	Bronze
$Cs_{1.75}[Pt(CN)_4]\cdot xH_2O$	Cs(def)TCP	—[e,78]	2.88	~ 25[141]	Bronze
$K_2[Pt(CN)_4](FHF)_{0.30}\cdot 3H_2O$	$KCP(FHF)_{0.3}$	*P4mm*[79]	2.918(1) and 2.928(1)	—[d]	Reddish-bronze[85]
$Rb_2[Pt(CN)_4](FHF)_{0.40}$	$RbCP(FHF)_{0.4}$	*I4/mcm*[64]	2.798(1)	1600[1] 2300[94]	Gold
$Rb_2[Pt(CN)_4](FHF)_{0.26}\cdot 1.7H_2O$	$RbCP(FHF)_{0.26}$	*C2/c*[80]	2.89	—[d]	Greenish-bronze[85]
$Cs_2[Pt(CN)_4](FHF)_{0.39}$	$CsCP(FHF)_{0.4}$	*I4/mcm*[65]	2.833(1)	2000[1] 1600[94]	Reddish-gold[85]
$Cs_2[Pt(CN)_4](FHF)_{0.23}$	$CsCP(FHF)_{0.23}$	*I4/mcm*[81]	2.872(2)	250–350[95]	Reddish-bronze[85]
$Cs_2[Pt(CN)_4]F_{0.19}$	CsCP(F)	*Immm*[82]	2.886(1)	—[d]	Reddish-gold[85]
$[C(NH_2)_3]_2[Pt(CN)_4](FHF)_{0.26}\cdot xH_2O$	$GCP(FHF)_{0.26}$	—[d]	2.90[84]	—[d]	Bronze
$[C(NH_2)_3]_2[Pt(CN)_4]Br_{0.25}\cdot H_2O$[83]	GCP(Br)	*I4cm*[g]	2.908(2)	11[83]	Bronze

II-3-2- Synthesis, structure, and properties of K*(def)*TCP

The chemical formula of the cation deficient potassium tetracyanoplatinate sesquihydrate is $K_{1.75}Pt(CN)_4.1.5H_2O$. It was reported that the compound can be synthesized using either a chemical or an electrochemical reaction. Williams et al. studied the chemical synthesis which consists of dissolving dipotassium tetracyanoplatinate ($K_2Pt(CN)_4.3H_2O$) into hot water acidified with sulfuric acid (H_2SO_4), then adding 20% hydrogen peroxide for oxidation:

$$8K_2[Pt(CN)_4].3H_2O + H_2SO_4 + H_2O_2 \xrightarrow{H_2O}$$

$$8K_{1.75}[Pt(CN)_4].1.5H_2O + 14H_2O + K_2SO_4 \qquad \text{Eq. 34}$$

After stirring, cooling and filtering, the $K_{1.75}Pt(CN)_4.1.5H_2O$ needle-shaped crystals form with a bronze color. The reported yield is 46% of the initial $K_2Pt(CN)_4.3H_2O$.

The electrochemical reaction was first reported by J. Miller. He used a 0.2M aqueous solution of $K_2Pt(CN)_4$ in an electrolysis cell including platinum anode and cathode, then he applied an electric potential of 1.5V. The reaction produced needle crystals of $K_{1.75}Pt(CN)_4.1.5H_2O$ and dihydrogen gas at the cathode following the two half-cell reactions:

$$1.75\,K^{+} + Pt(CN)_4{}^{2-} + 1.5H_2O \xrightarrow{H_2O} K_{1.75}[Pt(CN)_4].1.5H_2O + 0.25\bar{e} \qquad \text{Eq. 35}$$

$$2H_2O + 2\bar{e} \rightarrow H_2 + 2OH^{-} \qquad \text{Eq. 36}$$

The structure of the cation-deficient partially oxidized tetracyanoplatinate (K*(def)*TCP) was fully studied by Williams et al. using single crystal neutron diffraction method. The crystal has a triclinic unit cell with cell parameters a=10.360Å, b=9.303Å, c=11.832Å, α=77.57°, β=114.75° and γ=73.64°.

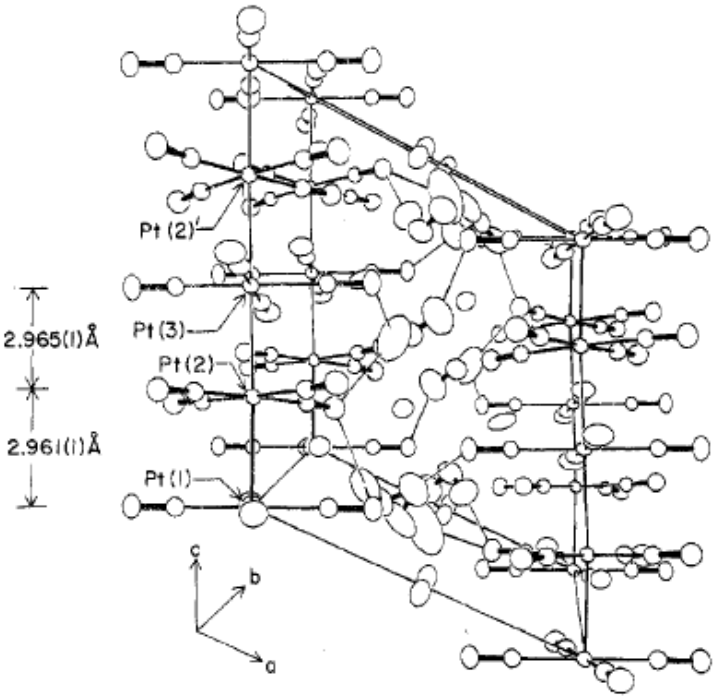

Figure 10- The unit cell of K(def)TCP showing the nonlinear Pt chain[5]

The unit cell comprises a zig-zag in the platinum chain with a bond angle of 173.25° between Pt(1)-Pt(2)-Pt(3) and a non-symmetric interatomic distances of 2.961Å and 2.965Å. The relatively short distance indicates a strong Pt-Pt metallic bond. The repulsive π-π cyanide interaction (negative charges of CN) creates a torsion angle between the consecutive tetracyanoplatinate groups. The torsion angle is between 38.46° and 51.82°, which deviates from

the equilibrium angle (45°). The zig-zag and the torsion angle deviation are the result of the asymmetric electrostatic interaction between the potassium ion and the cyanide group (K^+---$^-$N-C-Pt(2)). The water hydrogen bonding serves to maintaining the structure of the crystal by cross-linking the $Pt(CN)_4^-$ chains.

According to the reported studies, the produced K(def)TCP crystals have a needled-shape along the c-direction of the unit cell (parallel to the platinum chain) with a bronze color. The electric conductivity of the crystals is ~100 $\Omega^{-1}.cm^{-1}$ along the c-direction. The conductivity is lower than other anion-deficient KTCP, such as $K_2Pt(CN)_4Br_{0.30}.3H_2O$ (KCP-Br) which can reach ~1000 $\Omega^{-1}.cm^{-1}$. This is due to the relatively larger Pt-Pt distance in the K(def)TCP (2.96Å> 2.89Å) inducing a lower overlapping of the Pt d_z^2 orbitals. The crystals can lose water molecules easily, causing a degradation of the material since water hydrogen bonding is what keeps the platinum chains together. It needs to be stored over a saturated solution of NH_4Cl and KNO_3 with a relative humidity of 72% at room temperature.

II-3-3- Synthesis of K(def)TCP nanoparticles

L. Li[6] and P. Jahanian[7] obtained electrocrystallized K(*def*)TCP on highly oriented pyrolytic graphite (HOPG) upon the application of a potential pulse of 1.5V for 0.1s in 0.07 M of K2Pt(CN)4 in deionized water. The size range is of 0.6-5 µm in length and 0.1-0.5 µm in width, with an aspect ratio of 3.2 ± 0.9. When electrocrystallized on a gold nanoparticles (GNP) decorated HOPG, the morphology and the size of the K(*def*)TCP is highly dependent on the size of the GNP (Figure 12). It was observed that most K(*def*)TCP nanocrystals are oriented with their rod axis perpendicular to the seed/crystal interface while the rest are attached tangentially to the GNP surface, which suggests a preferential molecular attachment or nucleation direction of

the crystal on the GNP seed. The study showed that the seed-mediated electrocrystallization can be used to control the nucleation and growth of the nanorods.

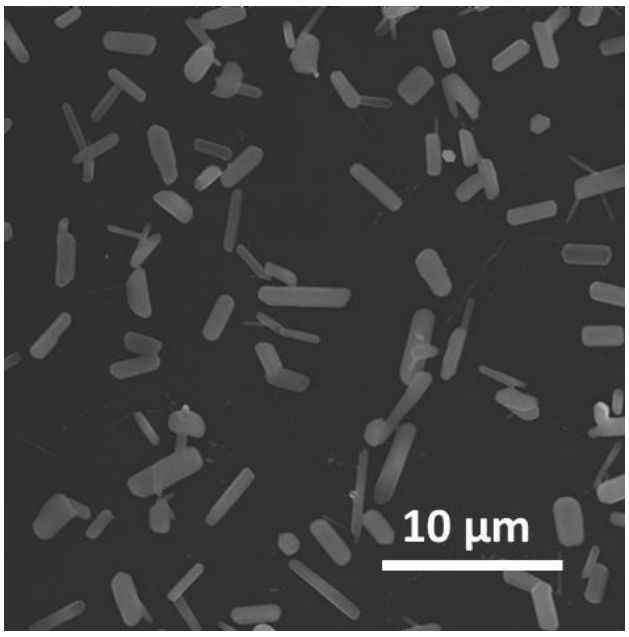

Figure 11- FE SEM image of K(def)TCP crystals electrochemically deposited on HOPG[7]

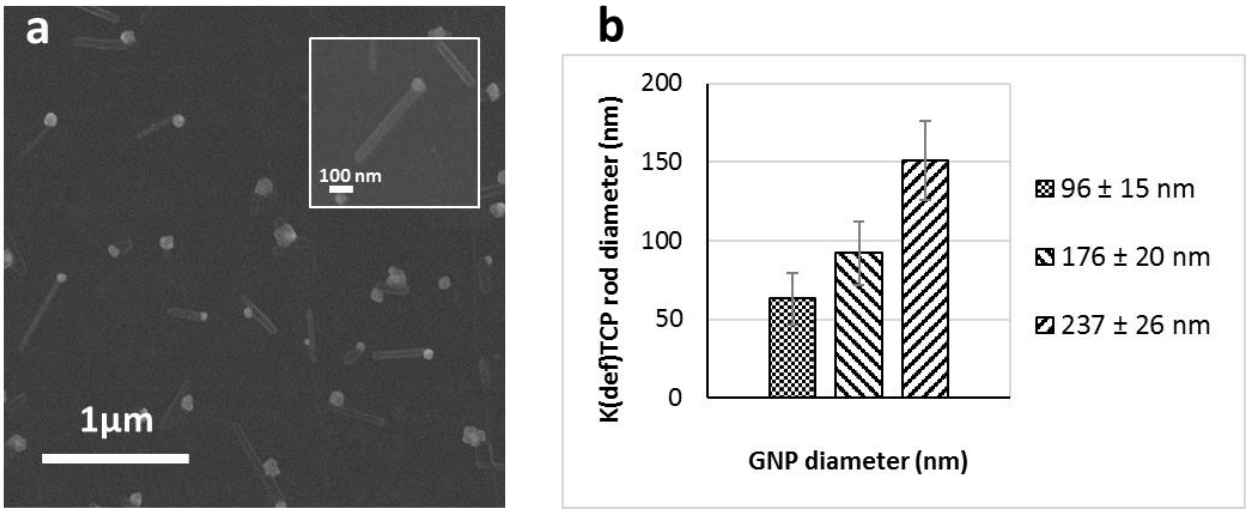

Figure 12- (a) FE SEM images of K*(def)*TCP crystals electrochemically deposited on GNP, (b) Average GNP diameter vs Average K*(def)*TCP diameter[7]

II-4- Morphology control of nanoparticles

The recent studies in nanotechnology showed the dependence of the nanocrystals properties on their size and shape. When the crystal has a size of ~1-100nm, its properties change significantly from those of bulk size, since their behavior is dominated by the quantum effects. For instance, gold is known with its unique yellow color. At the nanoscale, gold nanoparticles can have red or purple colors, which is caused by the confinement of the electrons with the size of the particles. The high surface to volume ratio of nanoparticles enables the control their interfacial reactivity. This property is used to produce effective catalytic materials and to enhance the sensitivities of the chemical sensors. The size of the nanoparticles influences many properties such as electrical conductivity, fluorescence, and magnetic permeability. This makes the size control of nanoparticles a great tool to tune the properties of matter.

The shape of nanocrystals has also an effect on their properties. When two nanocrystals have different shapes, the facets ratio of their surfaces is different. Each facet of the crystal has a unique surface energy and a chemical reactivity, which affects the overall interaction of the nanocrystal with its environment. Xu et al.[8] studied the effect of silver nanoparticle shapes on the specific reaction rate of styreneconversion. They showed that the rate of conversion over nanocubes is over 14 times higher than that on nanoplates and four times higher than that on spherical nanoparticles (Figure 13). This was explained by the fact that the catalytic activity on the {100} planes is higher than that on {111} planes. The shape change can affect the optical properties of nanocrystals. Chao[9] compared the extinction efficiencies between cubic and spherical LaB_6 particles. The spherical particles showed narrower spectrum for all sizes of particles, in the other hand, cubic particles had higher peaks especially for larger particle sizes.

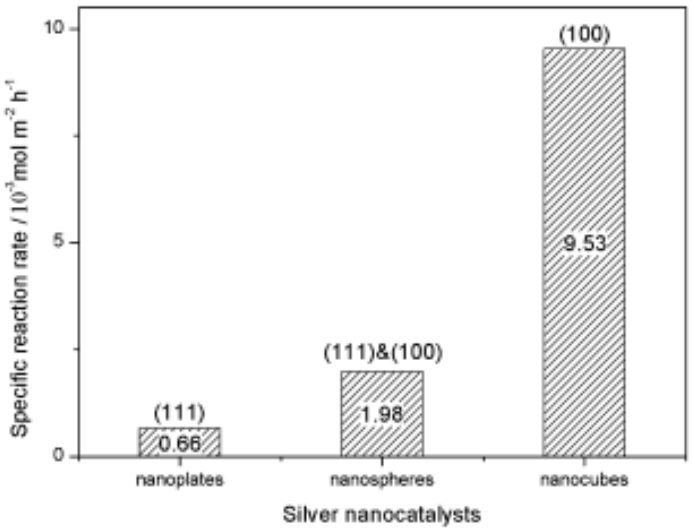

Figure 13- Specific reaction rate of styrene conversion over truncated triangular, near-spherical, and cubic silver nanoparticles. Reaction time: 3 h.[8]

Many recent works focused on how to control the shape and size of the particles and many strategies were established on the efficient way to master the properties tunability tool. Many classifications were presented on how to control the nucleation and growth of nanocrystals. We will present in this section the thermodynamic/kinetic classification approach. This approach is based on the competition between the different processes rates of the crystal formation (Diffusion, adsorption/attachment, hopping). As shown in the free energy scheme illustrated in Figure 14, The kinetic product (shape-I) is thermodynamically less favorable compared to the thermodynamic product (shape-II), because it has a higher free energy. However, when the atoms (or molecules) attach to the crystal, it is easier to overcome the energy barrier Ea_I (lower than Ea_{II}), which makes the reaction rate ($R = Ae^{-\frac{Ea}{kT}}$) of the kinetic product higher than the thermodynamic one. On the other hand, the adsorbed atoms tend to move to more thermodynamically stable positions (i.e. lower free energy). So, if the attachment rate is slower than the hopping rate, we will obtain an overall product more stable thermodynamically. The

thermodynamic/kinetic control can be achieved by changing the crystal formation parameters, such as temperature, concentration, surfactants, etc.

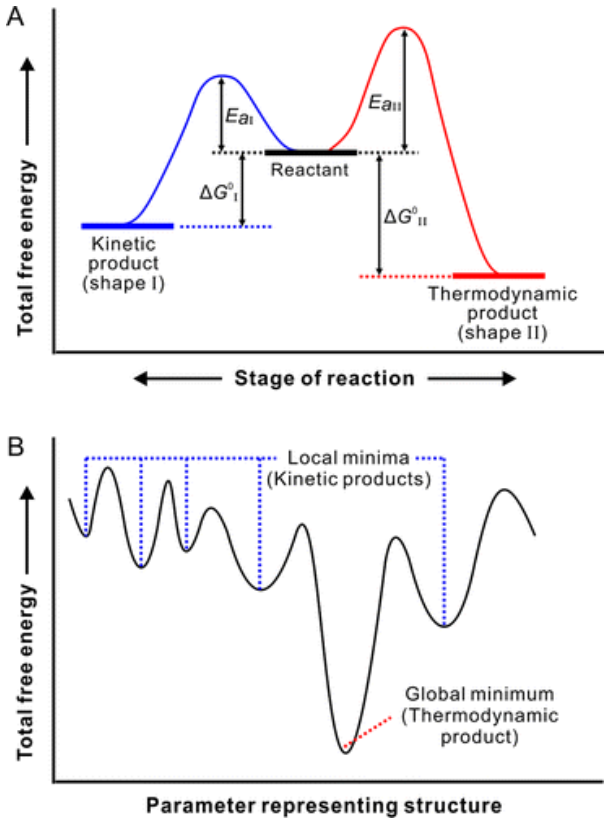

Figure 14- Schematic illustrations of two different scenarios of thermodynamic versus kinetic control that involve (A) two parallel reactions (B) a series of sequential reactions[10]

II-4-1- Thermodynamic control

The thermodynamic shape is obtained by increasing the relative ratio between atoms hopping rate and deposition (attachment) rate. This can be usually achieved either by keeping the crystal for a long time after deposition, slowing the deposition process or increasing the temperature. The deposition rate can be controlled by changing the driving force (concentration, electric potential, etc.).

In vacuum, the equilibrium shape is determined when the free energy of the crystal reaches its global minimum which leads to the Wulff construction (§II-1-3-). The Wulff shape depends on the relative surface energies, which depends on the crystal structure (Body-centered cubic, face-centered cubic, etc.). For example, using the Harkin's model (only bonds between nearest neighbors are considered) in the simple cubic structure the surface energies of the low index planes are related as follows: $\gamma_{111} = 1.225\,\gamma_{110} = 1.734\,\gamma_{100}$. This leads to a truncated cube exposing only {100} and {110} facets. Although the principle is simple, almost no experimental work could show the growth shape of nanoparticles in vacuum. Many computational works were done on the equilibrium shape in vacuum using density functional theory techniques. The major limitations of this method are its complexity, because it is very hard to get to the vacuum experimentally, and the limit of the shapes that you can produce since it depends only on the unit cell type of the crystal.

The generation of new shapes thermodynamically stable requires the change of the surface energy of the facets. This can be achieved by changing the chemistry of the surfaces. Adsorbates can be added to the surface which changes its interfacial energy, thus the ratio between facets and consequently the shape of the particles will change. Wang et al. showed that the growth of Pt nanocrystals in gas phase can produce different shapes depending on the gas nature. The gas molecules are adsorbed on the surface of the crystal. Depending on the adsorption sites, the gas molecules preferentially bind to certain facets. The adsorption reduces the facet surface energy, which changes the ratio between the exposed facets. Figure 15 shows the shape transformation of Pt nanocrystals grown on amorphous SiO_2 and Al_2O_3 in different gas phases. When grown in N_2 or air, the Pt nanocrystals tend to have a truncated cuboctahedron shape, while they transform into cubes when annealed in H_2 from dominantly {100} planes.

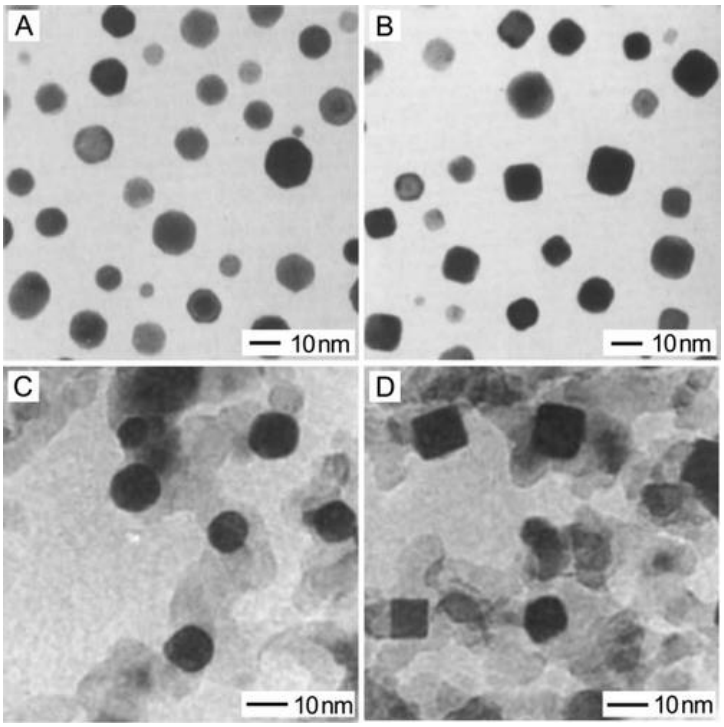

Figure 15- (A,B) TEM images of Pt nanocrystals supported on planar amorphous SiO2 after annealing under (A) N2 and (B) H2 at 600 °C for 24 h. (C,D) TEM images of Pt nanocrystals supported on Al2O3 powders after annealing (C) in air at 700 °C for 1 h and (D) under H2 containing a trace amount of H2S at 500 °C for 16 h.[11]

In a solution, a common technique for the control of the crystal shape is the use of capping agents[12]. Capping agents can be small molecules or polymers. Similar to gas molecules, they can selectively bind to specific facet types, reducing their surface energy, and permitting the change in the relative area ratio of the exposed facets. Kinetically, the phenomenon can be explained by the change in the relative rates of facets growth: the capping agents prevent the attachment of atoms to a specific facet which leads to a shape mostly expressed by that specific facet. Liao et al.[13] studied the growth of platinum nanocrystal facets under the transmission electron microscope (TEM), using a solution of oleylamine, oleic acid and pentadecane. The observations showed that the facets {100}, {011} and {111} had the same growth rate until the

size of the crystal reached 2.7nm, when {100} stopped growing before the other facets. Assisted with a DFT calculation, they showed that the amin group of the oleylamine molecule which functionalizes the Pt atoms on the surface prevents the atoms from binding on the {100} plane which reduces its deposition rate compared to the other two facets.

This method is widely used due to the variety of molecules binding selectively to different facets. Zeng et al.[14] showed how the shape of Ag nanocrystals can vary depending on the capping agent nature. They could selectively obtain Ag octahedrons enclosed by {111} facets and nanocubes enclosed by {100} facets by adding sodium citrate (Na_3CA) and poly(vinyl pyrrolidone) (PVP).

The concentration of the capping agent plays also a role in the determination of the final shape. With a high concentration, the capping agent can keep covering selectively the facet as the crystal grows. On the other hand, if the concentration is low, after a certain size, the capping agents cannot cover the entire crystal, especially on the edges, which permits the uncovered parts of the facet to continue growing[15].

II-4-2- Kinetic control

When the crystal is growing, there is always a competition between the deposition and the hopping (surface diffusion) processes. If the rate of deposition rate is higher than the hopping rate, the shape of the crystal will be trapped in a local minimum of the free energy, called the kinetic shape. The deposition rate increases with a higher concentration of the monomers (Figure 16), lower temperature (Figure 17), or an increase in the driving force.

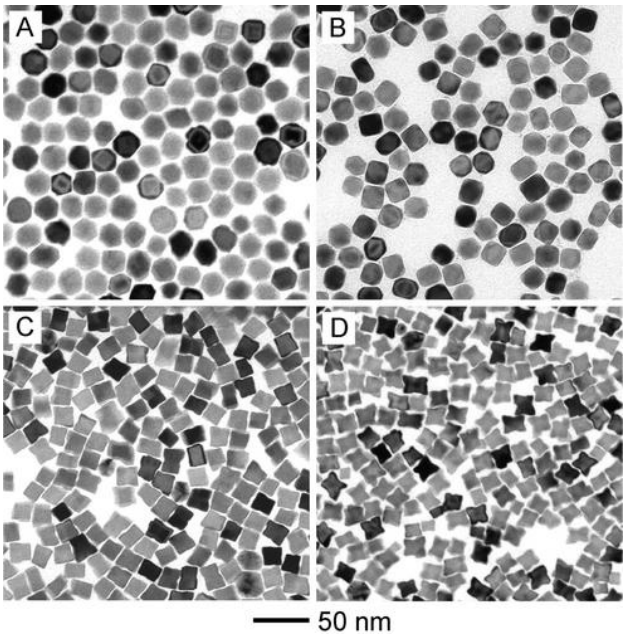

Figure 16- Palladium nanocrystals with four distinctive shapes that were obtained by injecting Na2PdCl4 solution into an aqueous suspension containing 15 nm Pd nanocubes, PVP, and ascorbic acid (22 °C) at different injection rates: (A) 0.25, (B) 0.5, (C) 0.75, and (D) 1.5 mL/h [16]

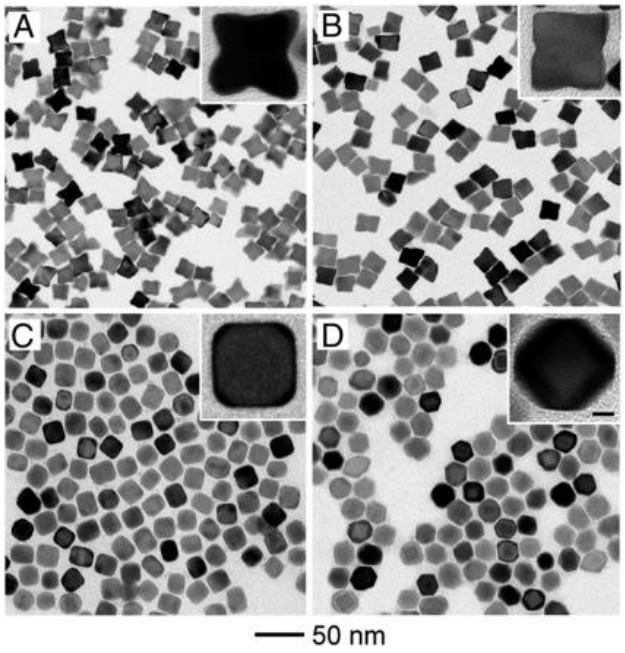

Figure 17- TEM images of Pd nanocrystals prepared at different reaction temperatures: (A) 0, (B) 22, (C) 50, and (D) 75 °C [16]

Many groups have applied the kinetic control of shapes of nanocrystals in solutions. The technique is based on the use of low concentrations of the capping agents so that some parts of the surface will not be covered. When the deposition rate is fast, the monomers will accumulate on the uncovered parts, which creates new shapes with higher free energy (concave nanocubes, stars, etc.).

One of the interesting aspects of the kinetic growth of nanocrystals is the asymmetric shapes. When the crystal is intrinsically anisotropic, it has some structural defects, the deposition pattern is asymmetric or the seeds aggregate/attach during the growth, its final shape tends to be asymmetric, deviating from the symmetry imposed by the unit cell. A good example of intrinsically anisotropic growth of nanocrystal is CdSe[17]. Controlling the growth kinetics of wurtzite CdSe, it is possible to make nanocrystals with an aspect ratio ranging from unity to ten along the (0001) direction. The 1-D growth behavior is essentially due to the polarity of the crystal: along the (0001) direction, the crystal is essentially composed of an electropositive layer rich of Cd and a more electronegative Se-rich layer. The polar charge distribution leads to higher growth rate. When the concentration is low, due to the ripening effect the surface diffusion rate is higher than the deposition rate, which leads to a nearly spherical shape. For high concentrations of the monomer, the result is a rod-like shape along the c-axis. The phenomenon is confirmed for similar semiconductors such as, ZnSe, ZnO and CdS[18].

Crystal twinning is one of the defects that can lead to an anisotropic growth of the crystal. When the nuclei are formed, it happens that two of them share some of the same unit lattice points in a symmetric manner. The most interesting type of twinning is the multiple-twin which produces particles with shapes such as decahedron and icosahedron. This type of particles induces a strongly anisotropic growth behavior that can be used to produce 1-D crystals. The

mechanism responsible of the creation of the twin defects is still not well understood, which makes it difficult to implement intentionally for shape control.

Asymmetric shapes can be obtained with the attachment of small particles to form a bigger crystal. The mechanism was first introduced by Banfield[19], who studied the growth mechanism iron-oxidizing bacteria under the HR-TEM. The study revealed that 2-3 nm particles move and aggregate in a manner that adapts their structure orientations. The interaction between the particles can range from van der Waals to electrostatic which constitutes the driving force for the self-assembly. The mechanism was used to produce semiconductor quantum rods and nanowires[20–23].

Another technique that gets a lot of attention recently is the seed-mediated growth (or catalyst assisted growth). The reacting compounds in the solution produce a solid phase (crystal). A nanoparticle acts as a catalyst for the reaction, thus the supersaturation of the reaction product starts a heterogeneous crystallization on top of the nanoparticle, creating a confined crystal shape. Using gold nanoparticles as catalysts, this method was used to grow semiconductor nanorods of Ag_2S[24] and CdS[25]. Recent studies showed the growth of organometallic nanorods on gold nanoparticles using electrocrystallization[26]. The results suggest that the aspect ratio of the tetrathiafulvalene (TTF) can be controlled by varying the size of GNPs.

III- Experimental methods

III-1- Electrochemical setup

The electrochemical procedure was performed using a Gamry potentiostat (PCI4/G300). A three-electrode cell was used for the electrocrystallization, where the working electrode (WE) is the substrate (HOPG), the counter electrode (CE) is made of Pt (0.25mm) and the reference electrode (RE) made of Ag, are immersed in the solution droplet. The working-sense lead is connected to the working electrode, and the counter-sense lead is connected to the counter electrode. In this study, we used both amperometry and potentiometry. The electrochemical station is connected to a computer to visualize the measurement data.

III-2- Atomic force microscope

The atomic force microscope (AFM) is an instrument that belongs to the scanning probe microscopy family. After inventing the scanning tunneling microscope (STM), Gerd Binnig and Heinrich Rohrer developed the AFM at IBM in 1982. It is one of the most powerful tools for the surface characterization at the nanoscale. The AFM is composed mainly from a laser generator, photodetector (position detector), cantilever, and a feedback loop controller. The cantilever, attached to a holder, has a sharp tip at its end. Its dimensions are typically in the micrometer scale. It is usually made of silicon. The tip is the sensitive part, and it is on the scale of a few nanometers. When the tip touches the surface of the studied sample, the cantilever bends. The reflected laser recorded with the photodetector deviates. The measured deviation is used to measure the bending force. The controller acts on a piezoelectric actuator to change the height of the cantilever until the force returns to zero.

The AFM has usually two imaging modes, contact mode and tapping mode. In the contact mode, the tip is touches the surface of the sample continuously while scanning. The change in the measured force (or deflection) is converted to height, which gives a topographical image of the surface. The contact mode can also be used to measure the surface state depending on the interaction with the tip. In the tapping mode, the cantilever oscillates (alternating bending) with a frequency near from its resonance frequency. When the tip encounters a new height, the signal provided by the photodetector will deviate from the reference set point (error signal), so the controller will act on the piezoelectric actuator to move and recover the amplitude of the oscillation in order to have a zero-error signal. This action will be seen as a “pulse” signal in the amplitude and a change in the height.

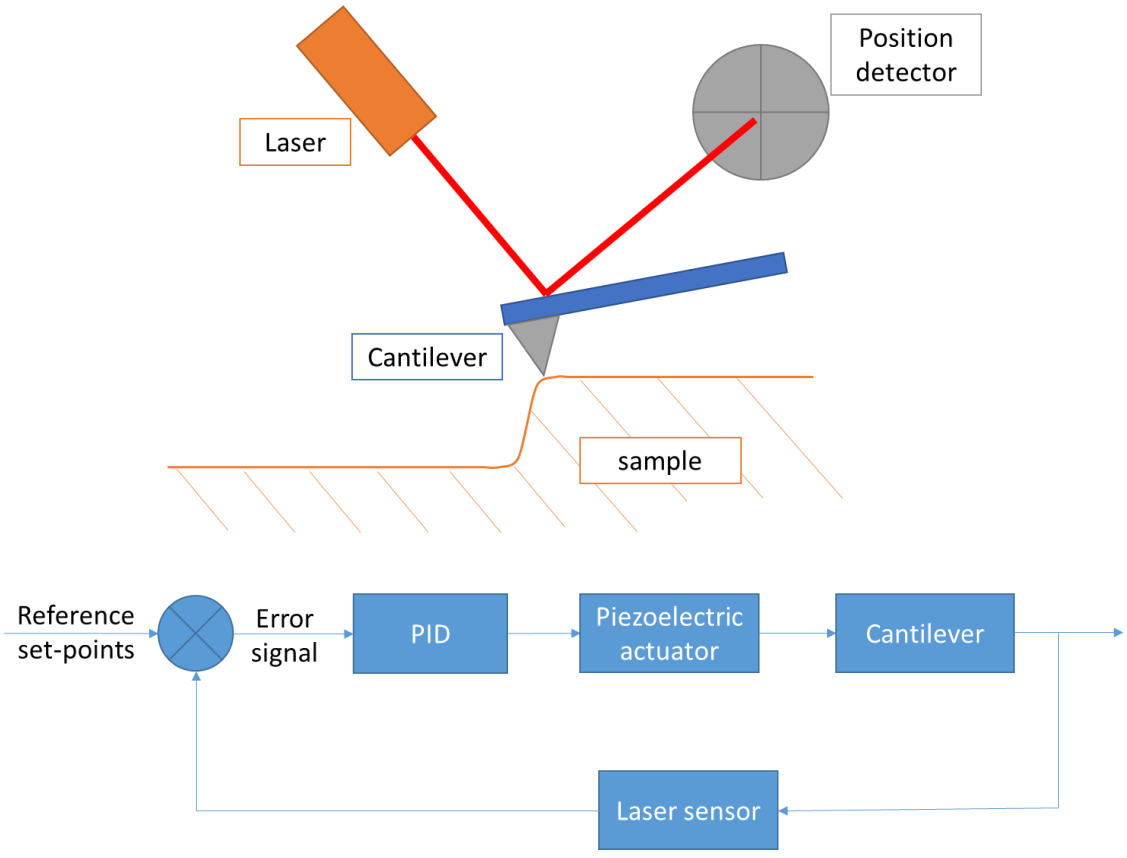

Figure 18- Illustration of an AFM

In this work, we used the Brucker- Dimension 3100 AFM. We used the tapping mode in air for the imaging of the K(def)TCP nanoparticles. The cantilever is made of silicon, oscillated at a frequency of ~300kHz.

III-3- Field emission Scanning Electron Microscope

The field emission scanning electron microscope (FE-SEM) is an imaging tool that uses a focused beam of electrons to scan a sample. When the electrons hit the sample, they interact with the atoms, and they produce signals that are detected and processed. Depending on the depth and the type of interaction, the produced signals can be secondary electrons, back-scattered electrons, X-ray and light photons, absorbed current and transmitted electrons. The FE-SEM can provide topographical and elemental information with a high special resolution (less than 1nm) with relatively lower voltage which minimizes the damage and charging of the smaple.

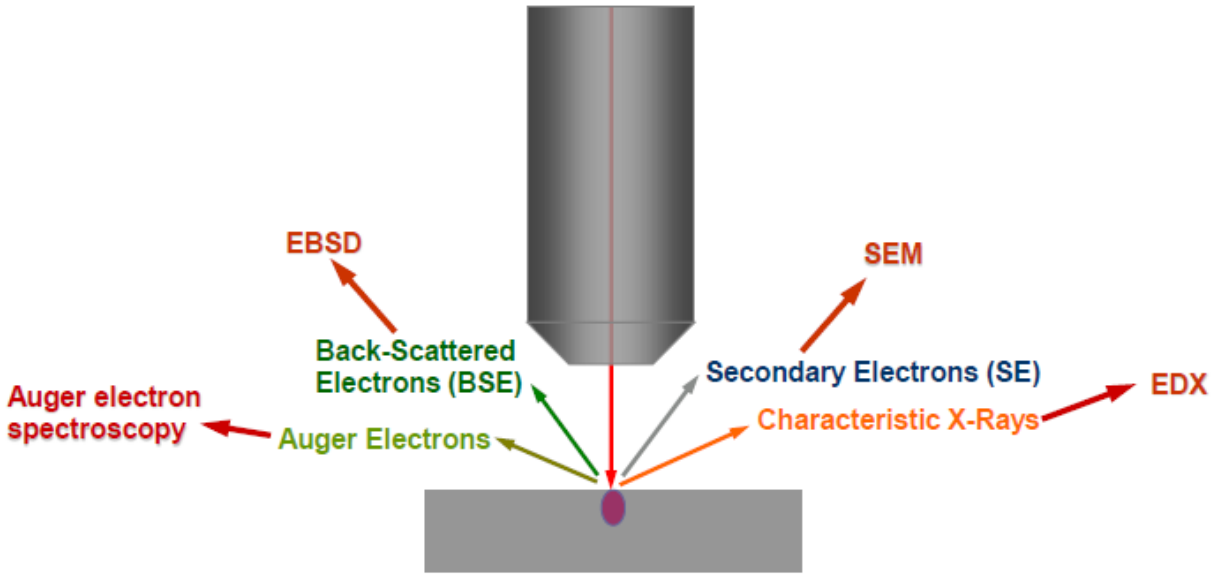

Figure 19- Illustration of an FE-SEM

In this study, we used the JSM-7600 FE SEM in the chemistry department of Wayne State University. The samples didn't need any coating since they are conductive. The imaging was performed in high vacuum.

III-4- Materials studio simulations

Materials studio is a software tool used for materials modeling and simulation that was developed by Accelrys (now distributed by BIOVIA). The software includes a set of toolbox that can be used to model and visualize crystal structures, optimize chemical structures, calculate the bond energies, predict crystals morphologies, and analyze XRD data.

In this study, we used the software to reconstruct the K(def)TCP structure, calculate its electronic structure and predict the thermodynamic shape of the crystal with Castep (DFT calculation tool).

IV- Electrocrystallization of potassium tetracyanoplatinate nanocrystals

IV-1- Introduction

Organometallic structures are applied to nanotechnology. Nanocrystals of the Krogmann salts are attractive nanomaterials due their platinum chain that offers unique 1-D properties. Experimental studies showed that charge transfer salts nanocrystals have different growth behavior compared to those of the bulk, when electrochemically synthesized[26]. This suggests that we can control the growth conditions to produce nanocrystals of desired shapes.

As we discussed in chapter-2, the morphology control of nanoparticles is possible by changing the experimental parameters to switch between the thermodynamic and kinetic shapes. The use of electrocrystallization for nanoparticles synthesis presents notable advantages compared to other nanofabrication techniques. It is easier, highly selective, and offers a flexible control over the growth conditions by tuning the electrochemical parameters.

In this chapter, the experimental results of the growth control via electrocrystallization are presented. A preliminary study shows the chemical and electronic structure of K(def)TCP as well as the thermodynamic shape predicted by DFT calculations on Materials Studio (Castep). The morphological transitions were studied upon changing the applied potential, the current and the concentration of the electrolytic solution. The results will be discussed and an experimental strategy for the morphology control of K(def)TCP nanocrystals will be presented at the end of the chapter.

IV-2- Crystal structural study of K(def)TCP

The structural data of K(def)TCP was based on the work of William et al.[5,27] K(def)TCP has a triclinic unit cell with parameters a=10.360Å, b=9.303Å, c=11.832Å, α=77.57°, β=114.75°

and γ=73.64°.The structure was reproduced on Materials Studio to reexamine the structure and the bonding.

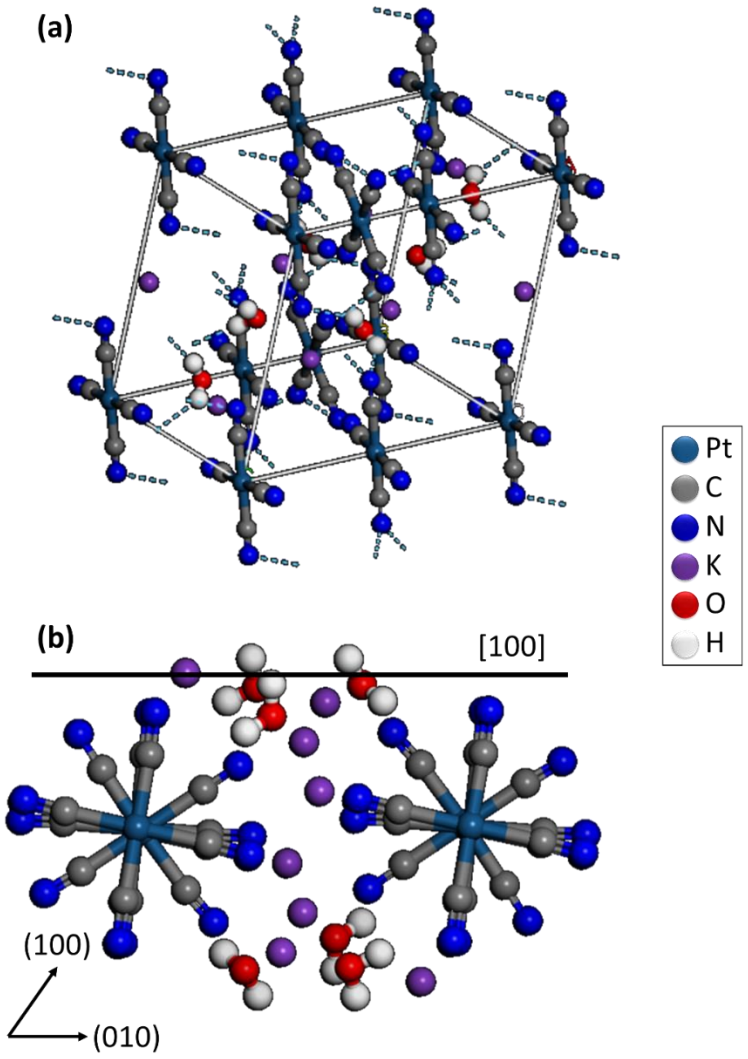

Figure 20- Structure of K(def)TCP reproduced on Materials Studio (a) Unit cell, (b) Section of the crystal along (001) direction

The analysis of the electronic and chemical structure of K(def)TCP was performed using a DFT calculation on Castep. The Generalized Gradient Approximation of Perdew–Burke–Ernzerhof exchange-correlation functional was used with a cut-off energy of 300eV.

The electronic distribution (Figure 21) shows the overlapping of the Pt d_z^2 orbitals which confirms the electric conductivity along the Pt chain. The overlapping disappears for electron densities higher than ~0.28 e/Å^3. The density in the direction perpendicular to the Pt chain is very low which means that the electric conductivity in those directions is lower than the one parallel to the c-axis. The calculations agree with the experimental observations.

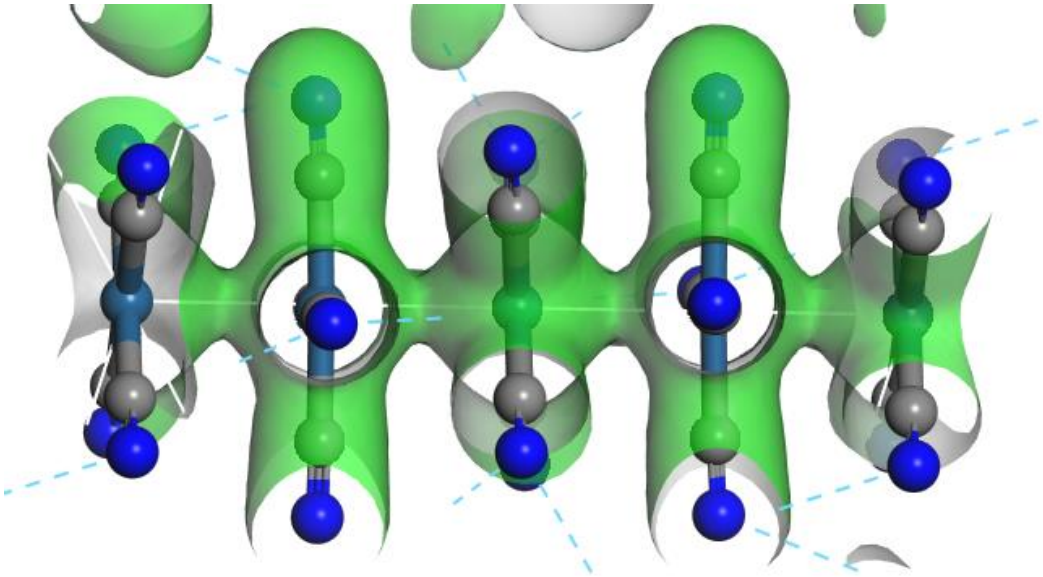

Figure 21- Isosurface of the electron density of 0.2e/Å3

The band structure calculated with a separation of 0.025 Å^{-1}. The density of states show the band structure of K(def)TCP. The calculated band gap between the conduction and valence bands is 0.572eV. The energy gap value is between 0.1eV and 3eV, which reveals the semi-conductive nature of K(def)TCP.

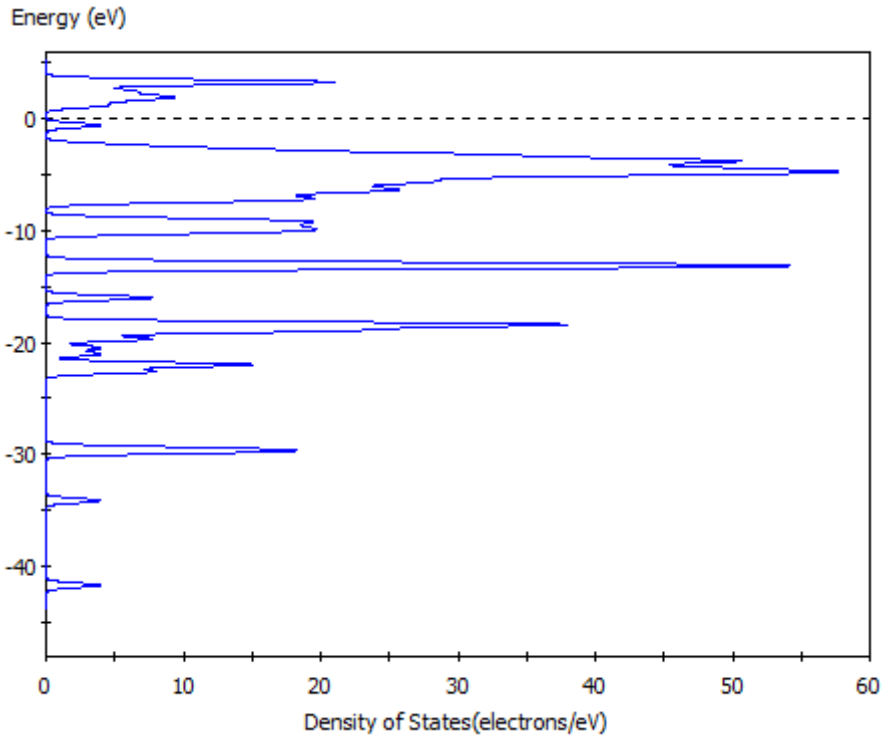

Figure 22- Density of states of K(def)TCP

The morphology of the crystal was predicted with Morphology tool. Bravais-Friedel Donnay-Harker (BFDH) method was used to generate the facets list. The BFDH method uses the symmetry of the unit cell to generate the list of possible growth faces and their relative growth rates[28]. The model does not take the bonding energy into account, but serves as a good approximation for the growth behavior prediction.

The shape is more isotropic and does not show the shape that was reported previously. The calculated shape is not a 1D shape. Table-2 shows the percentage of the exposed facets on the crystal surface.

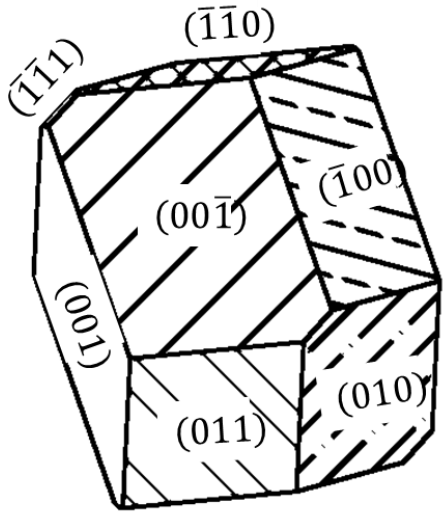

Figure 23- Crystal shape produced by the BFDH method

Table 2- Percentage of the apparent facets on the crystal

Facet {h k l}	**% Facet**
{0 0 1}	24.45
{1 0 -1}	20.67
{0 1 0}	15.86
{1 0 0}	13.58
{1 1 0}	12.60
{0 1 1}	11.97
{1 1 -1}	0.87

IV-1- Cyclic Voltammetry

Two aqueous solutions of 0.07M and 0.2M of $K_2Pt(CN)_4.3H_2O$ (KTCP) were prepared in DI water. The growth of K(def)TCP was performed through the oxidation reaction (Eq. 35):

$$1.75\,K^+ + Pt(CN)_4{}^{2-} + 1.5H_2O \xrightarrow{H_2O} K_{1.75}[Pt(CN)_4].1.5H_2O + 0.25\bar{e}$$

Cyclic voltammetry (CV) measurements were used to determine the range of potentials that are appropriate for the electrocrystallization of K(def)TCP. Figure 24 shows the CV curves for the electrocrystallization on HOPG in KTCP solutions with concentrations of 0.07M and 0.2M between -0.5V and 1.5V. The scan rate is 50mV/s with a step size of 1mV.

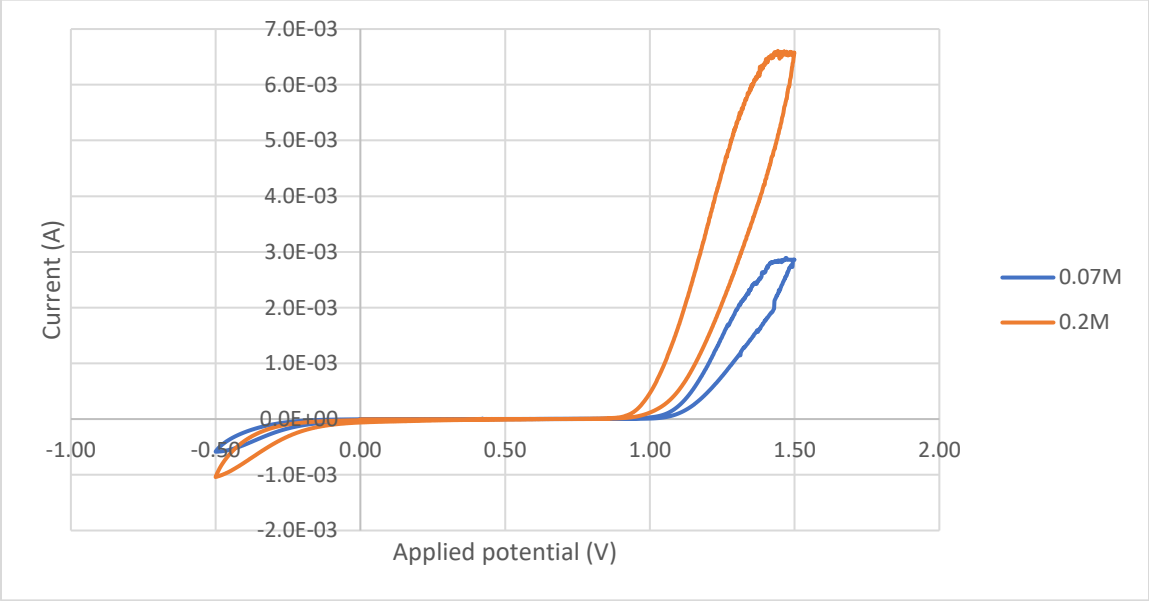

Figure 24- CV curves in 0.07M and 0.2M KTCP solutions on the HOPG electrode

The equilibrium potential E_{eq} is ~0.4V for the concentration of 0.07M and ~0.63V for 0.2M at room temperature. The cathodic current indicates that the electrocrystallization reaction is happening for applied potentials higher than the transition potentials E_{tr} of 1V and 0.85V for the 0.07M and 0.2M solutions respectively. For potentials between E_{eq} and E_{tr}, the current is relatively low, which means that the charge transfer rate is low. For potentials higher than E_{tr}, the current increases dramatically. By applying the thermodynamic/kinetic transition, we can predict that for potentials between E_{eq} and E_{tr} the electrocrystallization of K(def)TCP is governed by the thermodynamic equilibrium, whereas for potentials higher than E_{tr}, the electrocrystallization is controlled with the kinetic behavior of the crystal growth.

The concentration of the solution also influences the reaction regime (thermodynamic/kinetic). Inversely to the concentration effect on the equilibrium potential, the increase of the solution concentration shifts E_{tr} to lower values.

IV-2- Effect of the applied potential on the crystal shape

We applied three potentials (0.5V, 1V, 1.2V) on 50µl KTCP droplet and a freshly cleaved HOPG, for two different concentrations (0.07M, 0.2M) and a deposition time of 1 second. In this section, we are interested in the effect of the applied potential on the crystal growth of K(def)TCP.

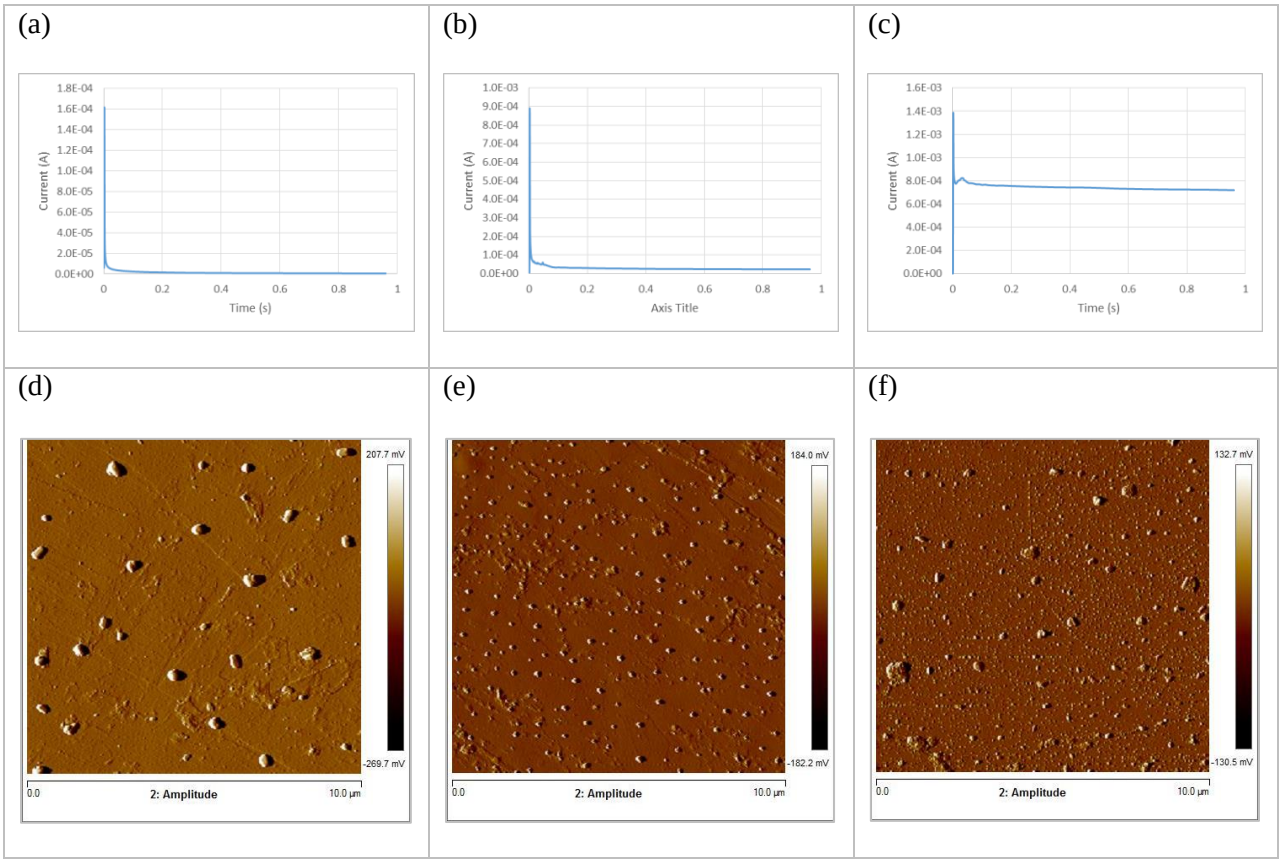

Figure 25- Effect of the applied potential on the K(def)TCP crystal shape electrocrystallized in 0.07M KTCP solution in 1s (a-c) the current behavior for applied potentials of (a) 0.5V, (b) 1V and (c) 1.2V. (d-f) AFM images for applied potentials of (d) 0.5V, (e) 1V and (f) 1.2V

Figure 25 (a, b, and c) shows the evolution of the cathodic current during electrocrystallization. The curves show a relatively large peak in the beginning of the deposition, which represents the instantaneous nucleation process. These observations are in agreement with previously reported results[29–31]. This means that the higher the peak, the greater the number of the created nuclei. The AFM images (from left to right) show that when the applied potential increases (the current peak increases as well), the density of the nuclei increases.

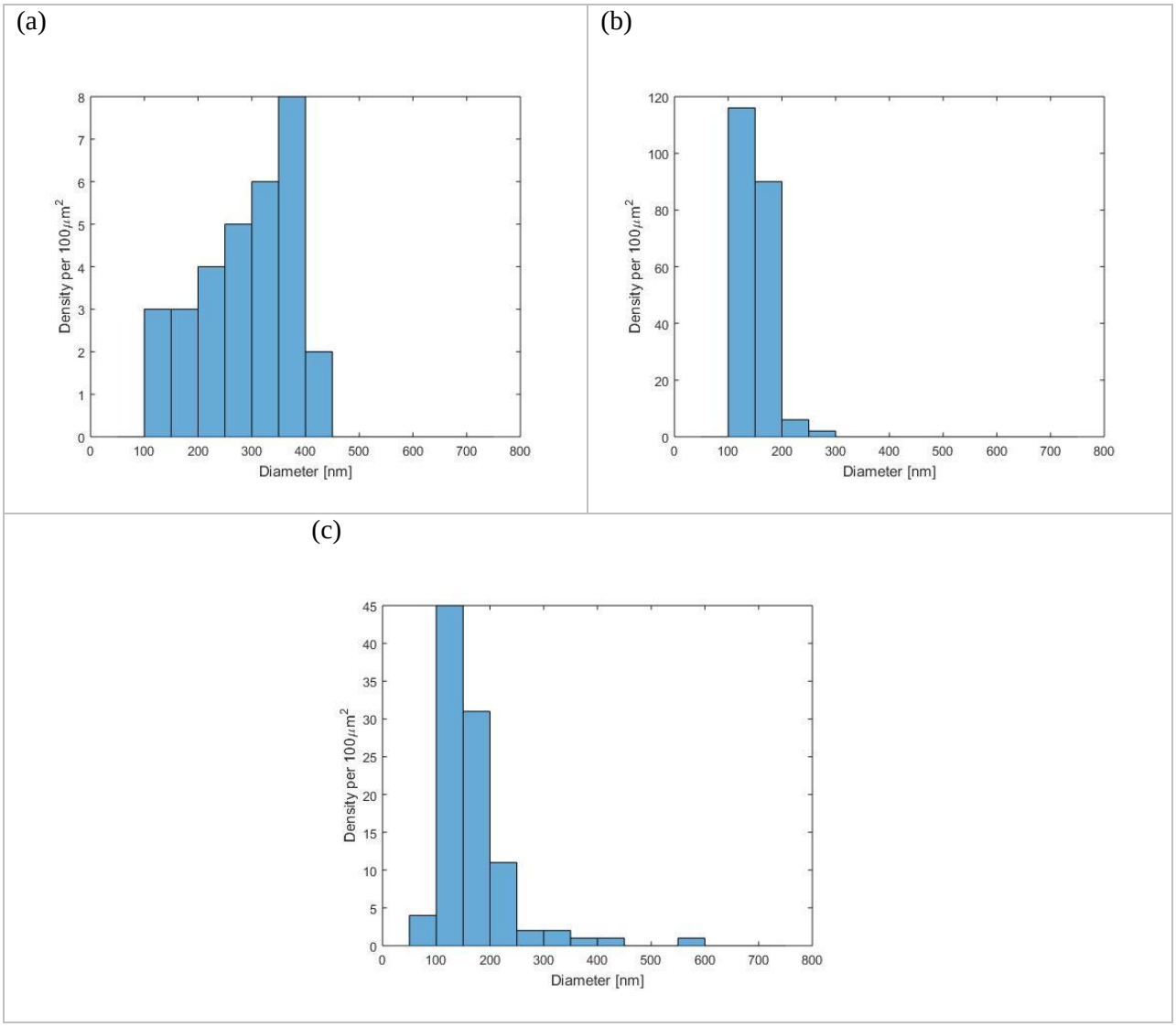

Figure 26- Particle size distribution of electrocrystallized K(def)TCP in 0.07M KTCP during 1s in an applied potential of (a) 0.5V, (b) 1V and (c) 1.2V

The size of the crystals depends on the applied potential. For an applied potential of 0.5V (Figure 25-d), the density of particles is ~0.3μm^{-2}. The particles have spherical shapes with diameters ranging between 118-422nm (Figure 26-a) with an average of 286nm and a standard deviation (STD) of 87nm. When the applied potential is 1V (Figure 25-e), the number of nanocrystal increases significantly (density of particles ~2μm^{-2}), but the size of particles decreases having an average of 150nm and an STD of 29nm (size range between 100-292nm). For an applied potential of 1.2V (Figure 25-f), the density of particles is ~1μm^{-2} with an average size and an STD of 167nm and 73nm respectively. The 1.2V electrocrystallization produces relatively larger range of sizes (85-600nm).

The transition between 0.5V and 1V agree with the nucleation and crystal growth theory. For low potentials (i.e. low overpotential), the driving force is low, which limits the nucleation frequency. During the growth stage, the deposited molecules will be distributed on a limited number of nuclei and the crystals reach relatively larger sizes. This is probably due to lower energetic cost of crystal growth compared to nucleation. When we increase the applied potential (0.5→1V), the number of nuclei becomes larger since the driving force is high and allows more nuclei to overcome the nucleation energy barrier. The deposited molecules need to be distributed on a larger number of nuclei, which keeps the size of the formed crystal small compared to those formed with 0.5V. We expected to have a similar trend going from 1V to 1.2V, instead, the particle distribution show a lower density for 1.2V and particles with bigger sizes. The AFM images (Figure 25-f) show that the big particles are agglomerates of small crystals. this is due to a higher driving force which increases the nucleation frequency and causes the formation of small nuclei, which assemble to form polycrystalline particles with dendritic shapes.

Figure 27 confirms the dependence of the K(def)TCP growth behavior on the applied potential. We applied 1, 1.2 and 1.5V on 0.2M of KTCP solution. The cathodic current response (Figure 27-a, b, and c) is similar to what we had with 0.07M: the current has a peak in the beginning proportional to the applied potential. The dependence of the current value on the solution concentration will be discussed in the next section.

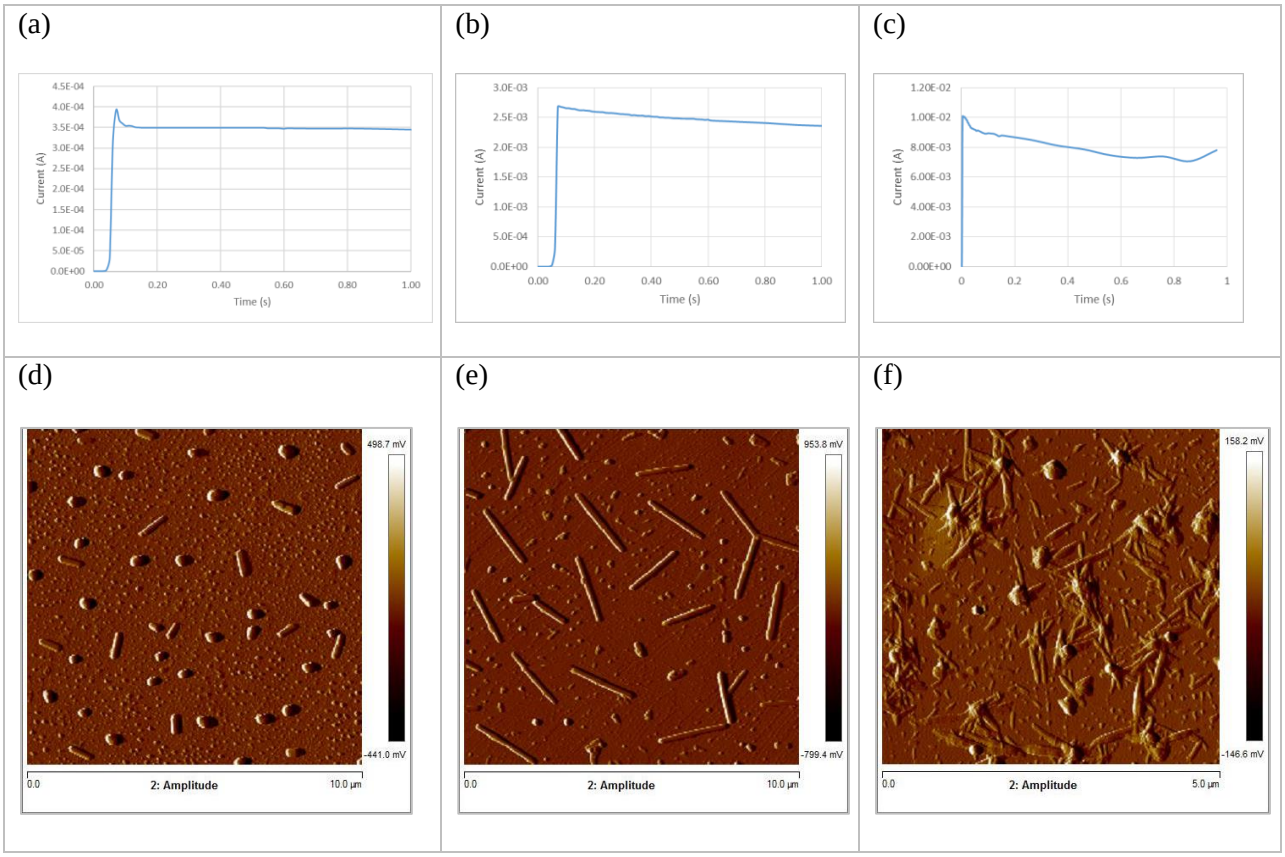

Figure 27- Effect of the applied potential on the K(def)TCP crystal shape electrocrystallized in 0.2M KTCP solution in 1s (a-c) the current behavior for applied potentials of (a) 1V, (b) 1.2V and (c) 1.5V. (d-f) AFM images for applied potentials of (d) 1V, (e) 1.2V and (f) 1.5V

The increase of the applied potential increases the number of crystals. The density of particles with 1V is ~0.5µm^{-2} while it becomes ~1µm^{-2} with 1.2V. This again agrees with the

nucleation theory and shows that the nucleation frequency increases when the overpotential increases. The crystals shape reveals a more interesting phenomenon. With 1V (Figure 27-d), we notice that the shape of some crystals tends to be elongated with sizes ranging between 150-850nm. The majority of the crystals have an aspect ratio (length to width) of ~1 (Figure 28-b). The elongated crystals (nanorods) have aspect ratios between 2-8. When the applied potential is increased to 1.2V (Figure 27-e), the density of the nanorods increases and we start to see longer shapes (aspect ratio between 2-16). The crystals have a wide range of sizes (120-2300nm). The small crystals correspond to newly nucleated particles. With a potential of 1.5V (Figure 27-f), we notice the presence of three types of shapes: spherical, elongated and star-like shape. The star-like shaped particles correspond to the agglomeration of the elongated and sphere particles. The quantitative analysis of the electrocrystallization behavior for 1.5V was not possible because of its complexity.

As to our knowledge, this behavior is reported for the first time for this type of crystals. These observations show that the potential has not only an influence on the nucleation density of crystals, but also the growth behavior.

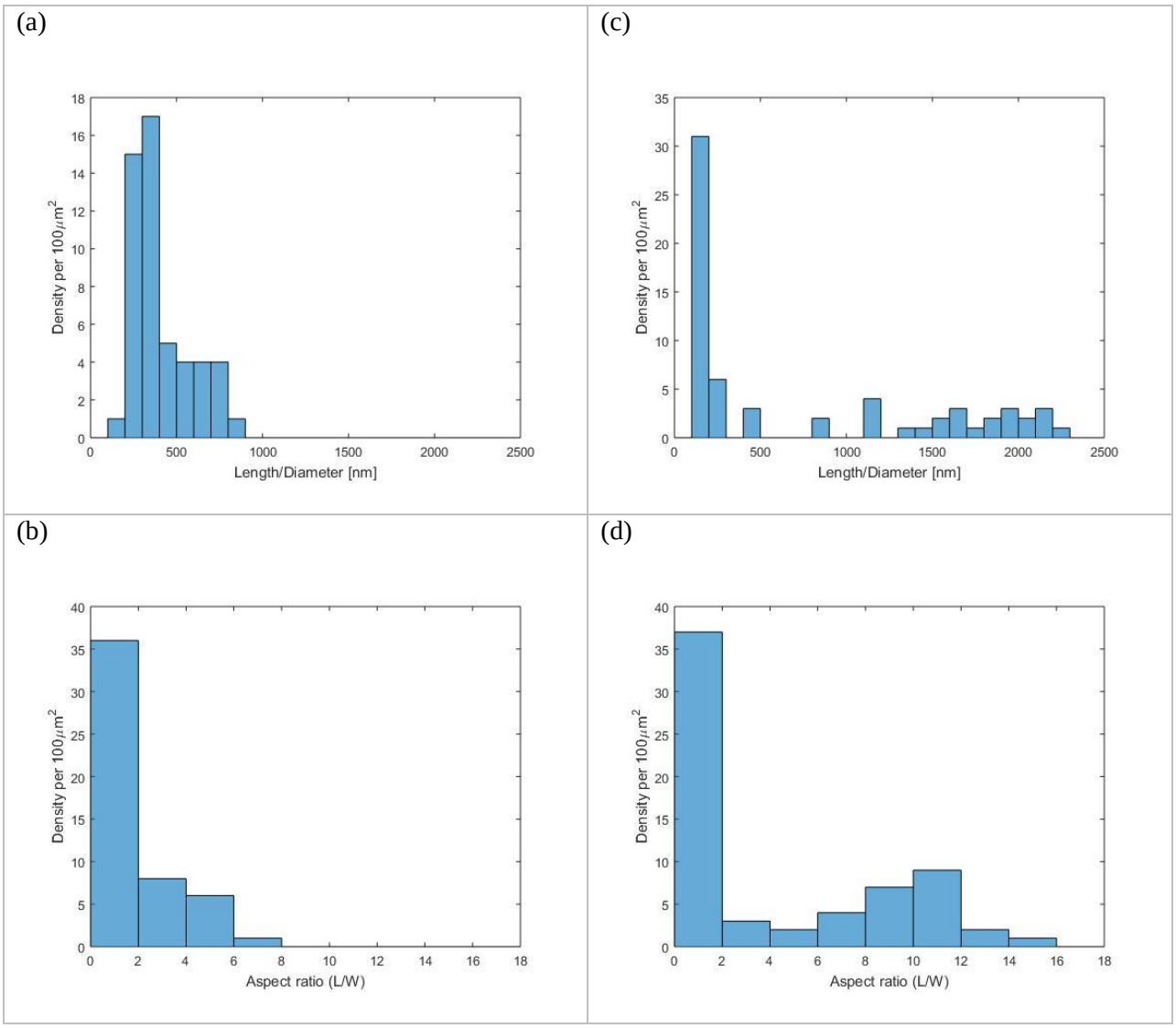

Figure 28-Particle size and aspect ratio distributions of electrocrystallized K(def)TCP in 0.2M KTCP during 1s in an applied potential of (a,b) 1V and (c,d) 1.2V

IV-3- Effect of the concentration

As we saw in the CV curves, the change in the concentration changes the current for the same applied potential, this indicates that the rate of the reaction is also changing.

The AFM images in Figure 29 show that the concentration influences the density and the shape of the formed crystals. For low concentrations, we see only spherical crystals, while for high concentrations, rod shapes appear. These observations suggest that the crystal morphology

can be controlled by changing the concentration. An increase in the concentration increases the aspect ratio of the crystal.

	[KTCP] = 0.07M	[KTCP] = 0.2M
1.0V	(a) 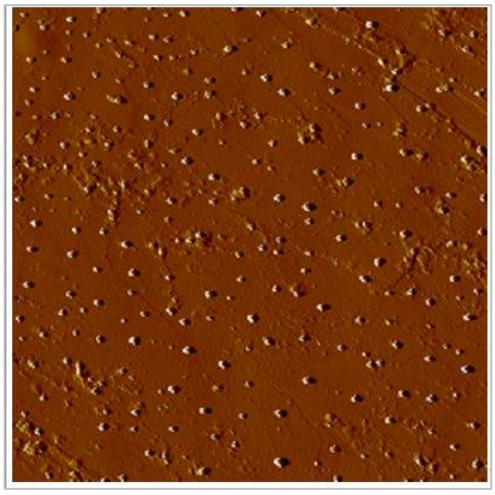	(b) 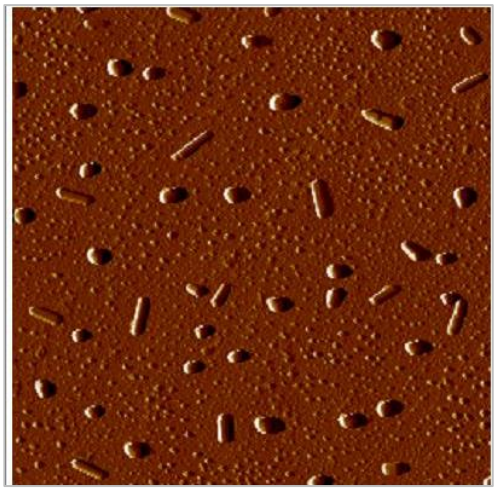
1.2V	(c) 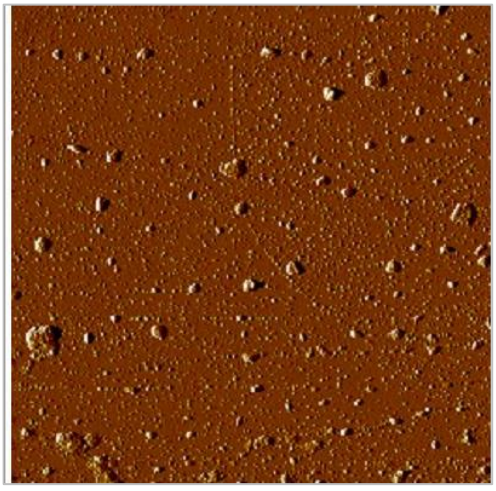	(d) 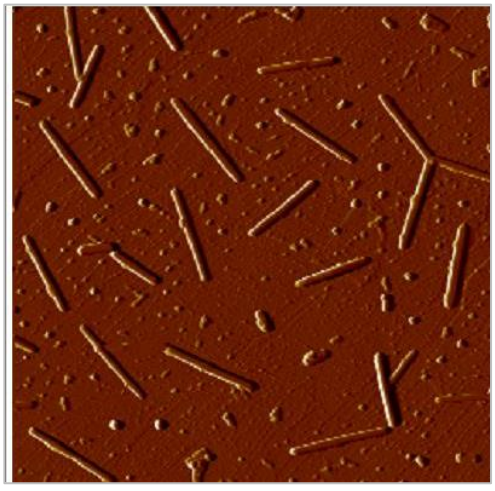

Figure 29- Effect of the solution concentration on the growth behavior

IV-4- Effect of the current

The AFM images in Figure 30 show the effect of the current on the crystals shape. Constant currents of 3mA and 6mA were applied on the 0.2M KTCP solution for 1s. The size of

the crystals is proportional to the applied current. The width of the crystals is almost the same for the two applied currents, which means that only the aspect ratio of the crystal is affected by the value of the current.

(a)

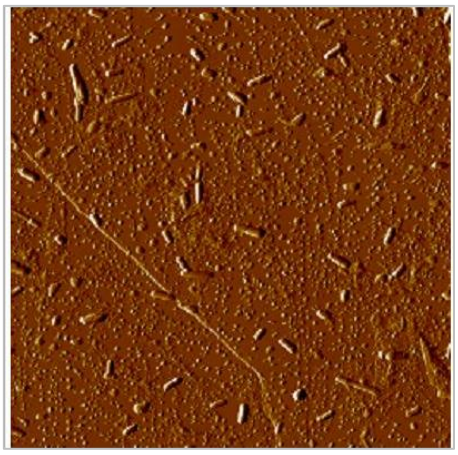

(b)

Figure 30- AFM images showing the crystal shapes electrocrystallized in a concentration of 0.2M in 1s for a current of (a) 3mA and (b) 6mA (square size is 10μm)

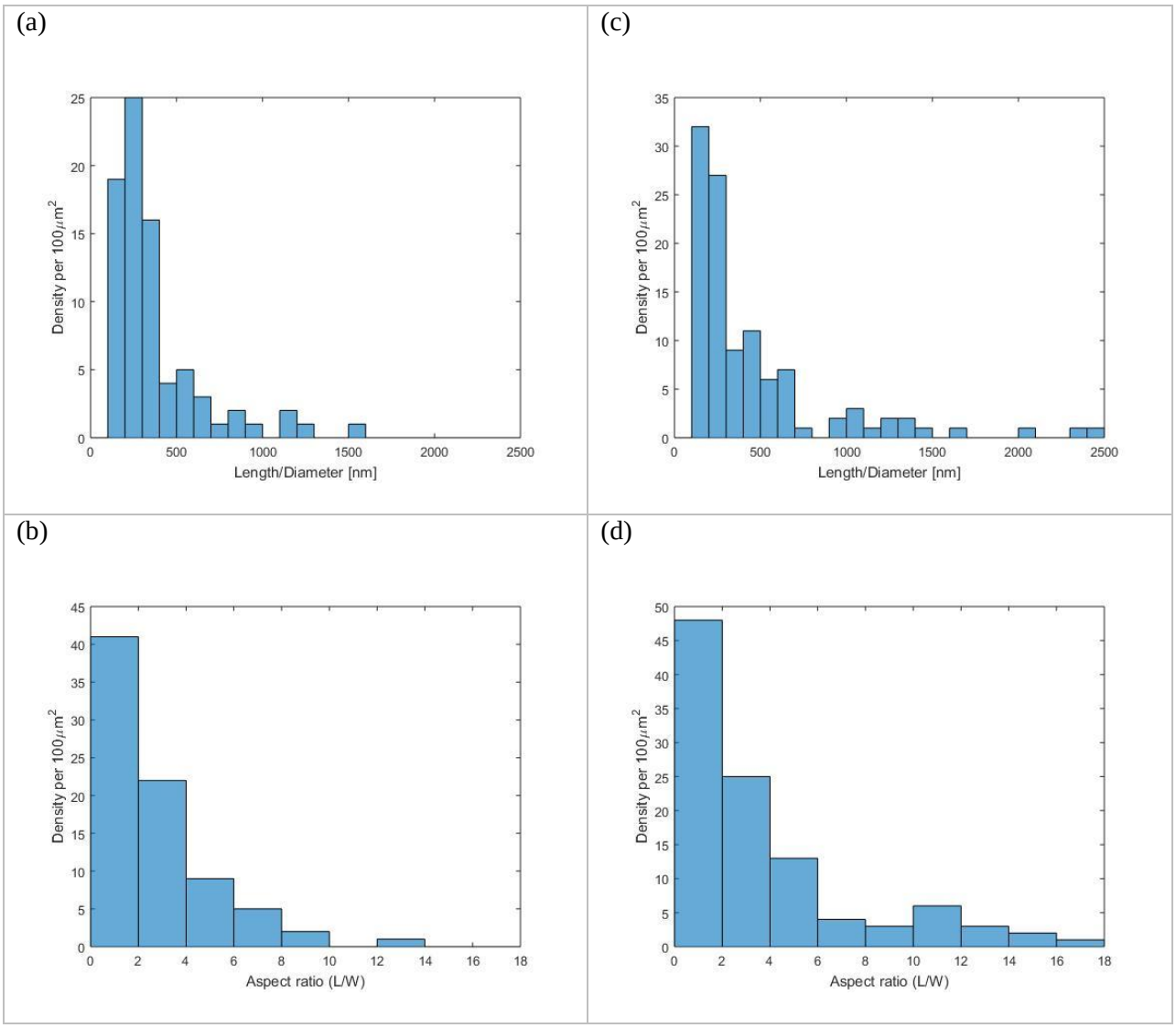

Figure 31- Particle size and aspect ratio distributions of electrocrystallized K(def)TCP in 0.2M KTCP during 1s in an applied current of (a,b) 3mA and (c,d) 6mA

In order to verify the trend of the K(def)TCP crystal growth, we realized the electrocrystallization for very low currents. For an applied current of 1nA during 1000s, the electrodeposited crystal has a rhombohedral shape very similar to the one calculated by the BFDH method. The obtained particles have a very narrow size distribution of 200nm. The shapes were confirmed with an FE-SEM imaging. The nanoparticles have a depression on the top surface. The phenomenon is still not understood[32].

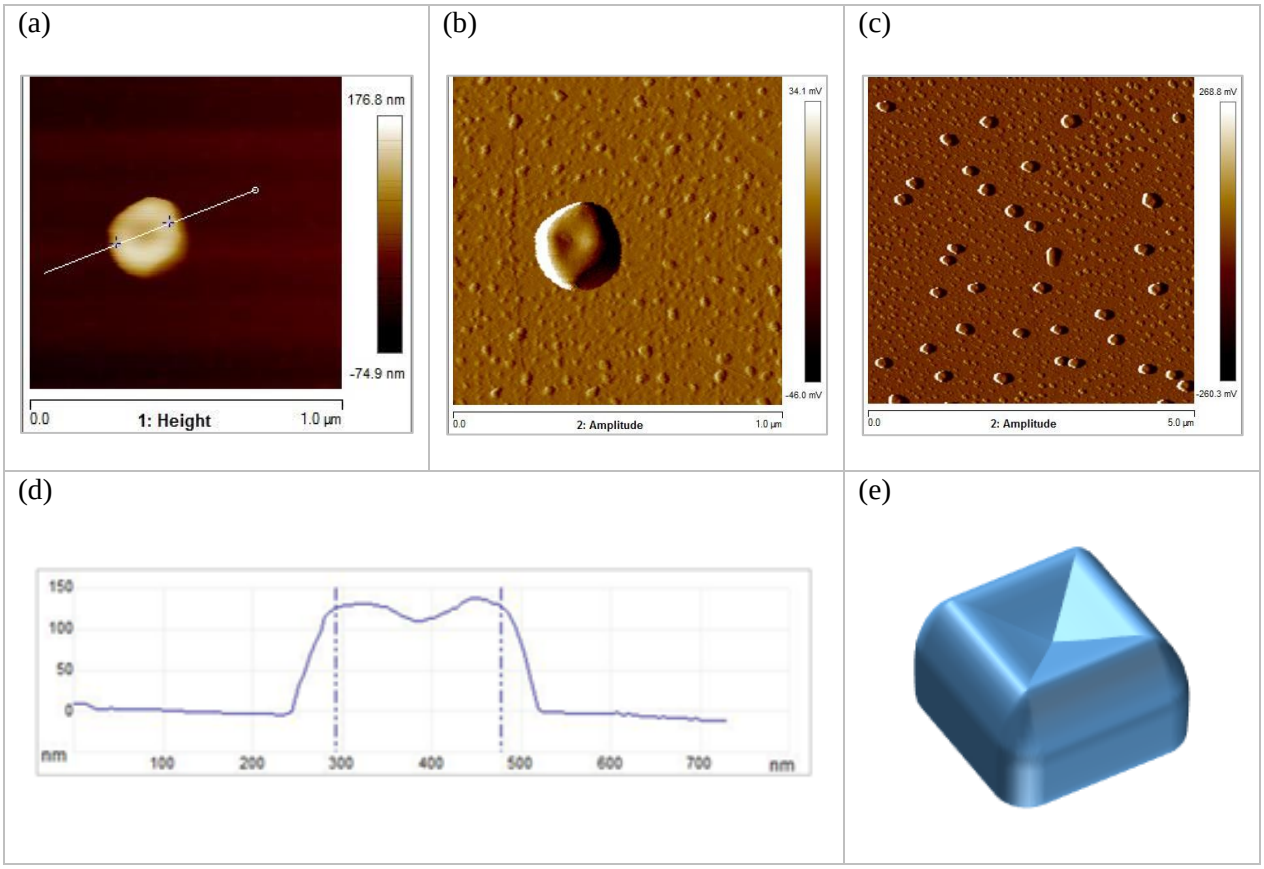

Figure 32- K(def)TCP nanoparticle grown with a current of 1nA in 1000s. (a) AFM topography of the nanoparticle

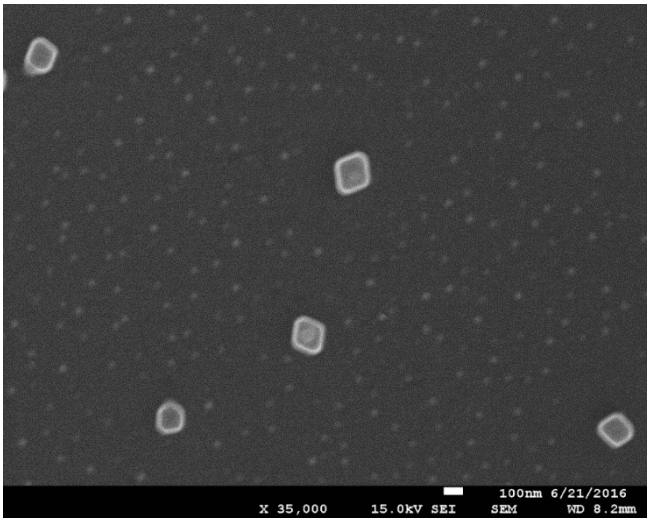

Figure 33- FE-SEM image of the rhombohedral shape

IV-5- Discussion and conclusions

All the above observations show that the electrical parameters and the concentration have a significant effect on the morphology of K(def)TCP crystals. The common parameter between all of them is the current, which can be related to the concentration and the overpotential by the Butler-Volmer equation:

$$i = i_0 \left(e^{\frac{\alpha z e \eta}{kT}} - e^{-\frac{(1-\alpha) z e \eta}{kT}} \right) \qquad \text{Eq. 37}$$

$$i_0 = kC^{\alpha} \qquad \text{Eq. 38}$$

The reaction rate R is proportional to the current:

$$R = \frac{i}{zeA} \qquad \text{Eq. 39}$$

Where A is the area of the electrode, e is the electron charge, z=0.25 for the K(def)TCP electrocrystallization reaction.

The shape of the crystals is also dependent on the kinetics of the electrochemical deposition. The following diagram shows a summary of the evolution of the crystals shape function of the different studied parameters (concentration, applied potential and current).

For low reaction rates, the crystals tend to form in rhombohedral shapes having a narrow size distribution. When we increase the reaction rate, the crystals tend to have a rod-like shape that has an aspect ratio (length/width) proportional to the reaction rate. Very high kinetics lead to the formation of agglomerates.

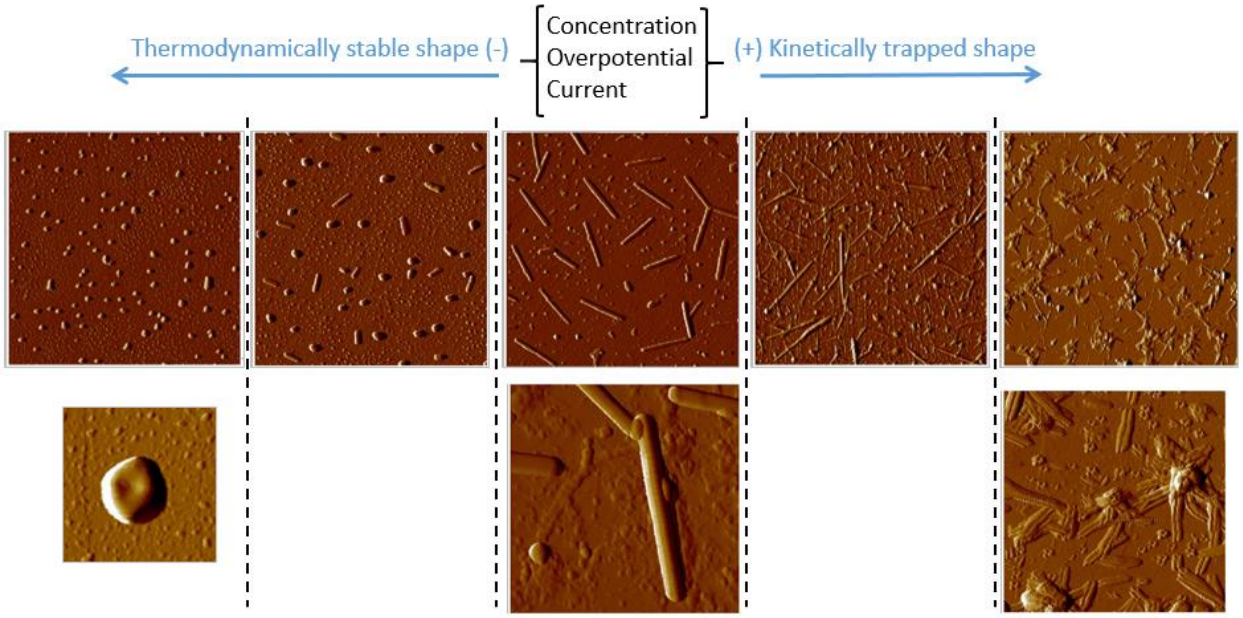

Figure 34- Thermodynamic/Kinetic control of K(def)TCP morphology

An alternative explanation suggests that the shape change can be explained by "Ostwald rule of stages". This means that crystals can be formed in many different phases (different crystalline structures) depending on the rate of the reaction: each shape is trapped in a local minimum of Gibbs free energy ΔG of the reaction. The most stable phase (corresponding to the global minimum of ΔG) is the rhombohedral shape, since it was produced with very low kinetics. Figure 35 illustrates the polymorphism of the KCP crystals as a function of the free energy and the reaction rate. This hypothesis can be verified by studying the crystal structure of each phase using the XRD for example.

This shape transition can be a good way for the engineering of nanoparticles, since it doesn't need any additives (e.g. capping agents) or mechanical control. The good understanding of the electrochemical theory is a main advantage because it helps to make a good prediction and control of the nanoparticles morphology. The explanation of the growth mechanism at the atomic

level is crucial to establish a better model for the phenomenon. This necessitate an in-situ characterization of the crystal growth.

We will present in the next chapter a model that can draw the relationship between the electrochemical parameters (concentration, current, applied potential) and the thermodynamic/kinetic morphology control.

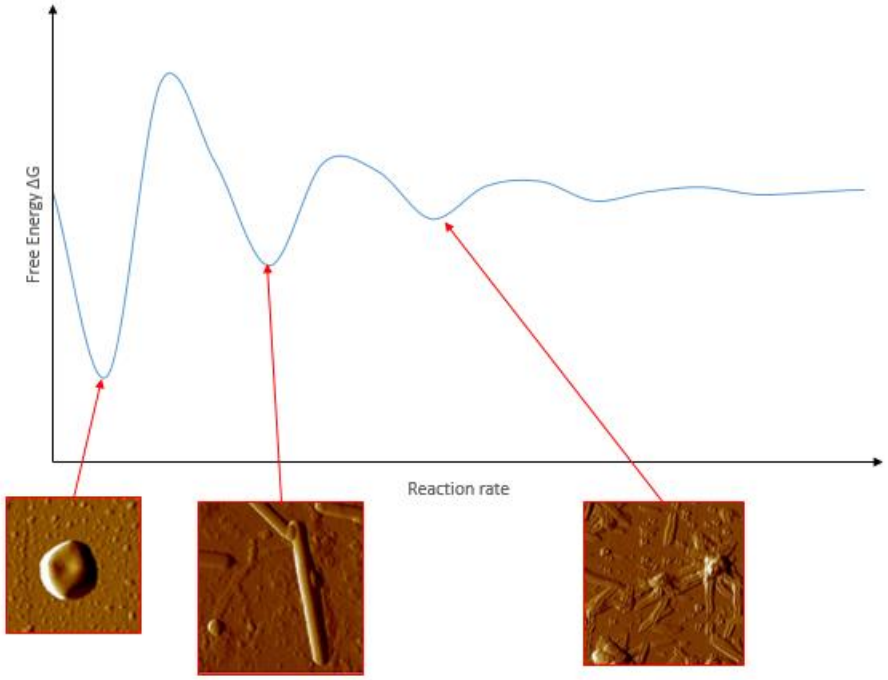

Figure 35- Illustration of the dependence of the crystal morphology on the reaction rate/free energy

V- Crystal growth modeling of K(def)TCP

The modeling of nanocrystal growth attracted many researchers to simulate its behavior[33–40]. The major challenge is to create a model that can take into account the effect of the thermodynamic and kinetic parameters, and to be able to switch between the different growth modes. Many techniques were employed to simulate the crystal growth, such as molecular dynamics[34,35,38], monte-carlo[39,41] and density functional theory[33,42]. DFT calculations are used to study the chemical interactions between the crystal atoms, and based on that it gives a thermodynamic approach for the crystal shape behavior. Molecular dynamics studies the physical motion of the atoms considering their interaction, and the shape of the crystal can be obtained from the quasi-equilibrium state of the atoms. Monte-Carlo is a stochastic simulation method that solves molecular interactions and motions based on the probability of molecular events, which leads to a statistical equilibrium.

We will present in this section a mathematical modeling of the growth behavior versus the thermodynamic/kinetic control in electrocrystallization. The model is an attempt to combine the thermodynamic model based on the Wulff construction and the kinetic model based on Butler-Volmer equation. The results of Monte-Carlo simulation will be presented to show the how can the mathematical model predict the crystals shape considering the growth anisotropy.

V-1- Mathematical model

The description of the crystal growth is usually described either from a thermodynamic point of view or a kinetic one. The thermodynamic description of the crystal growth is based on the notion of equilibrium described by Gibbs (dG=0). The main result of this approach is the Wulff construction which gives a direct relationship between the surface energies of the crystals

facets and their growth rate: The ratio of surface energies is equal to the ratio of their growth rate (Eq-15), which means that the growth rate of a facet is proportional to its surface energy:

$$R_i = A\,\gamma_i \qquad \text{Eq. } 40$$

On the other hand, the kinetics of crystal growth in electrocrystallization is described by the Butler-Volmer equation. The current is expressed function of the concentration and the overpotential. To simplify, we will not consider the mass-transfer effect, which means that the solution concentration on the electrode surface is equal to the concentration of the bulk. The electrocrystallization rate is proportional to the current (Eq-33), and can be written as:

$$R = \frac{kC^{\alpha}}{zeA}\left(e^{\frac{(1-\alpha)ze\eta}{kT}} - e^{-\frac{\alpha ze\eta}{kT}}\right) \qquad \text{Eq. } 41$$

The Butler-Volmer model describes the overall reaction kinetics. However, taking into account the chemistry of each of the crystal facets to be of different nature, the Butler-Volmer equation needs to be modified accordingly. The modification comes into effect after incorporating unique sets of values of parameters (α, K) in the Butler-Volmer relation which in turn brings forth different rate equation for each respective facet.

$$R_i = K_i C^{\alpha_i}\left(e^{\frac{(1-\alpha_i)ze\eta}{kT}} - e^{-\frac{\alpha_i ze\eta}{kT}}\right) \qquad \text{Eq. } 42$$

Where K_i and α_i are the proportionality factor and the charge transfer coefficient of the facet "i" respectively.

The combination of the thermodynamic and kinetic behavior should reflect the transition between both of them: at low kinetics (i.e. low values of concentration, overpotential and current), the obtained shape should agree with the Wulff construction and the growth rate of each

facet should be proportional to its surface energy, however, when the kinetics are high (i.e. high values of concentration, overpotential and current), the growth rate should correspond to the Butler-Volmer equation. The growth rate expression that we propose for this work is:

$$R_i = A\,\gamma_i + K_i C^{\alpha_i}\left(e^{\frac{\alpha_i z e \eta}{kT}} - e^{-\frac{(1-\alpha_i) z e \eta}{kT}}\right) \qquad \text{Eq. 43}$$

The relative growth rate between two facets i and j is:

$$\frac{R_i}{R_j} = \frac{A\,\gamma_i + K_i C^{\alpha_i}\left(e^{\frac{\alpha_i z e \eta}{kT}} - e^{-\frac{(1-\alpha_i) z e \eta}{kT}}\right)}{A\,\gamma_j + K_j C^{\alpha_j}\left(e^{\frac{\alpha_j z e \eta}{kT}} - e^{-\frac{(1-\alpha_j) z e \eta}{kT}}\right)} \qquad \text{Eq. 44}$$

The model includes the thermodynamic/kinetic transition of the growth rate. When the kinetics are low, the kinetic parts tend toward zero, and the rate ratio will be equal to the surface energies ratio. However, with a proper choice of the parameter A, when the kinetics are high, the overall growth rate ratio will be governed by the kinetic parameters. Figure 36 shows an example on how the rate ratio varies function of the concentration and overpotential. The growth rate ratio starts from the surface energy ratios $\frac{\gamma_1}{\gamma_2}$ and increases to higher values when we increase either the overpotential or the concentration.

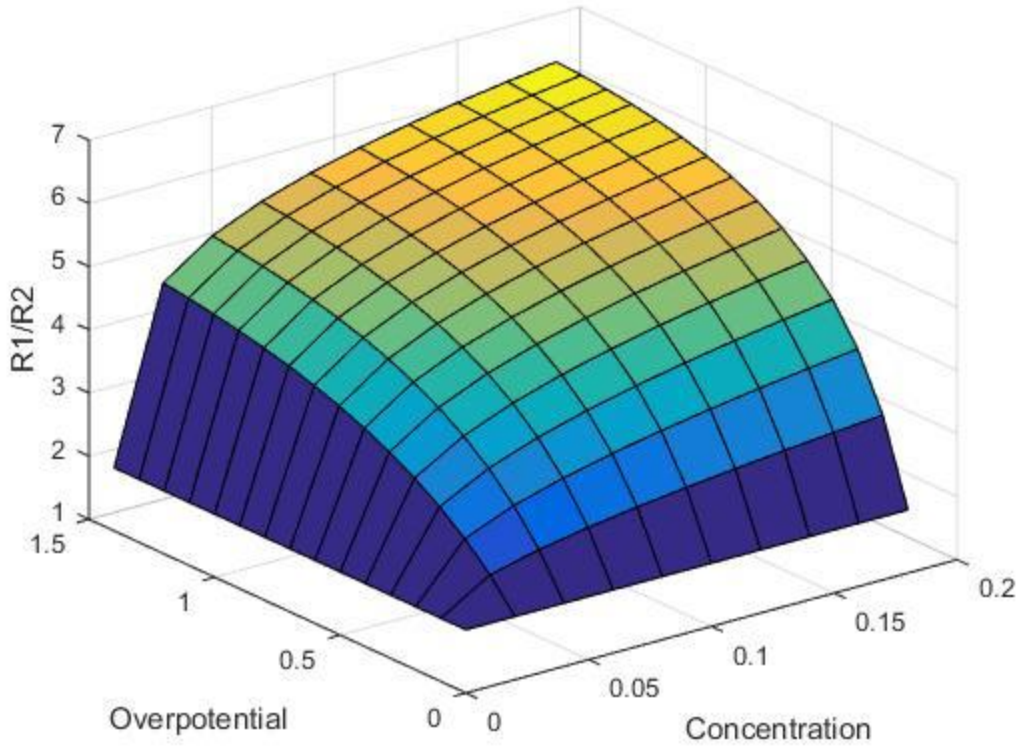

Figure 36- Variation of the growth rate ratio function of the concentration and the overpotential $\left(\frac{\gamma_1}{\gamma_2} = 2,\right.$

$$\left. K_1 = K_2 = 10,\ \alpha_1 = 0.49\ and\ \alpha_2 = 0.40 \right)$$

V-2- Monte-Carlo simulation

The Monte-Carlo simulations is a family of algorithms that uses random numbers to solve problems[43]. It is extensively used in chemistry to model the atoms motions and interactions through moving atoms by small random displacements. Each displacement is an event that has a probability, and it doesn't happen until it is higher than a random number.

The Monte-Carlo methods were used to simulate the crystal growth by electrocrystallization.[44–47] We present here a qualitative simulation of the growth behavior of K(def)TCP, based on the mathematical model and Monte-Carlo methods, to show the

thermodynamic/kinetic transition. The simulation takes into account the anisotropic properties of the crystal. The simulation space is represented with a 2-D grid, where each element corresponds to a position. The simulation starts with a nucleus in the middle of the grid. A deposition probability matrix is created to represent the deposition probability. The deposition probability is proportional to the rate of deposition. For simplicity, we will study only the growth of two facets. As shown in Figure 37, the deposition probabilities of the horizontal facets (1) are different from the vertical facets (2). The probabilities are calculated as follows:

$$P1 = \frac{R1}{2(R1 + R2)} \; ; \; P2 = \frac{R2}{2(R1 + R2)} \qquad \text{Eq. } 45$$

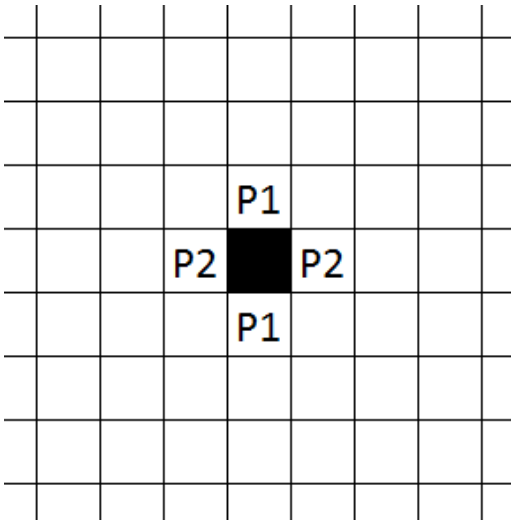

Figure 37- Simulation grid. The nucleus is represented with a black box, P1 and P2 are the respective deposition probability of facets 1 and 2

Figure 38 shows the results of the simulation for different values of concentration and overpotential. A 400x400 grid and 10^4 increments were used for the simulation. The model

parameters are $\frac{\gamma_1}{\gamma_2} = 2,\ K_1 = 2, K_2 = 1,\ \alpha_1 = 0.7\ and\ \alpha_2 = 0.51,$ where "1" and "2" refer to the vertical and horizontal facets respectively. The effect of the mass-transfer and surface diffusion are not considered. The simulation results show that the increase in the overpotential or the concentration increases the aspect ratio of the particle (length/width). These results are qualitatively in agreement with the experimental observations. The roughness of the shape edges is probably due to the absence of the surface diffusion.

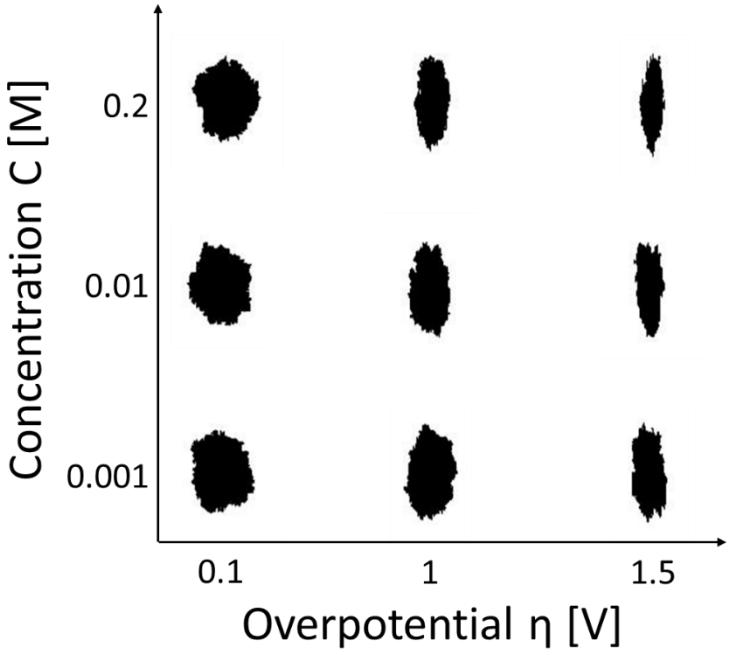

Figure 38- Monte-Carlo simulation results. The nanocrystal shape for different electrochemical conditions

VI- Conclusion and future work

This work discusses the experimental and theoretical methods used to control the morphology of nanocrystals. The hypothesis of the thermodynamic/kinetic control of the morphology was verified. We applied the electrocrystallization to make K(def)TCP nanocrystals and we tuned the electrochemical parameters to determine their influence on the nanocrystals morphologies. The characterization was mainly performed with AFM and FE-SEM. We presented in this work the possibility to control the morphology of K(def)TCP using the electrochemical parameters. The obtained shapes ranged from nanorods to rhombohedral shape, which is reported for the first time. The observed growth behavior was modeled and simulated with a method based on Monte-Carlo techniques. The simulation results show a qualitative match with the experimental findings.

This work confirms the thermodynamic/kinetic control hypothesis. We showed that the decrease in the kinetic parameters (applied potential, concentration and current) produces a rhombohedral shape with an aspect ratio close to one between the different facets. The crystal shape is similar to what was predicted by the BFDH calculation, which suggests that the rhombohedral shape is thermodynamically stable. The increase of the kinetic parameters increases the aspect ratio of the nanoparticles and produces nanorods. For very high kinetics, the nanocrystals form agglomerates.

The mathematical modeling of the growth behavior combined both thermodynamic and kinetics models. The growth rate of the crystal facets was written function of the surface energy, as in Wulff construction, and the Butler-Volmer model for electrocrystallization. The Monte-Carlo method was used to simulate the crystal behavior versus the electrochemical parameters

considering the anisotropy of the crystal properties. The simulation showed how the aspect ratio increases when the kinetics are high, which agrees with the experimental results.

This thesis contributes to the understanding of the crystal growth behavior and the thermodynamic/kinetic transition. We also combined the two growth regimes in a single model to simplify the behavior simulation.

Despite the important findings of this work, this thesis is only an introduction for a big experimental and theoretical work that can be done later. It can be extended to study the thermodynamic/kinetic transition with other charge transfer materials such as the other Krogmann salts and tetrathiafulvalene family. In situ characterization of the nanocrystals growth can provide a better understanding of the mechanisms.

References

(1) Wiley: Electrocrystallization in Nanotechnology - Georgi T. Staikov, 2017.

(2) Wiley: Electrochemical Methods: Fundamentals and Applications, 2nd Edition - Allen J. Bard, Larry R. Faulkner, 2017.

(3) Electrocrystallization - Fundamentals of Nucleation and | Alexander Milchev | Springer, 2017.

(4) Extended Linear Chain Compounds - Volume 1 | Joel Miller | Springer, 2017.

(5) Williams, J. M.; Keefer, K. D.; Washecheck, D. M.; Enright, N. P. *Inorg. Chem.* **1976**, *15*, 2446–2455.

(6) "Molecular Crystallization Directed By Nanoparticles And Nanopatterns " by Li Li, 2017.

(7) "Engineering Gold Nanoparticles And Their Use To Control Nucleation " by Pedram Jahanian, 2017.

(8) Xu, R.; Wang, D.; Li, Y.; Zhang, J. Shape-Dependent Catalytic Activity of Silver Nanoparticles for the Oxidation of Styrene. *Chemistry – An Asian Journal*, 2006, *1*, 888–893.

(9) Zhang, Z.; Tegus, O.; Chao, L.; Wei, W.; Bao, L. Effects of Nanoparticle Shape and Size on Optical Properties of LaB6. *Plasmonics*, *11*, 697–701.

(10) Xia, Y.; Xia, X.; Peng, H.-C. Shape-Controlled Synthesis of Colloidal Metal Nanocrystals: Thermodynamic versus Kinetic Products. *Journal of the American Chemical Society*, 2015, *137*, 7947–7966.

(11) Shape and orientation of supported Pt particles - ScienceDirect, 2017.

(12) Ling, D.; Boles, M. A.; Hyeon, T.; Talapin, D. V. The surface science of nanocrystals. *Nature Materials*, 2016, *15*.

(13) Liao, H.-G.; Zherebetskyy, D.; Xin, H.; Czarnik, C.; Ercius, P.; Elmlund, H.; Pan, M.; Wang, L.-W.; Zheng, H. *Science* **2014**, *345*, 916–919.

(14) Zeng, J.; Zheng, Y.; Rycenga, M.; Tao, J.; Li, Z.-Y.; Zhang, Q.; Zhu, Y.; Xia, Y. Controlling the Shapes of Silver Nanocrystals with Different Capping Agents. *Journal of the American Chemical Society*, 2010, *132*, 8552–8553.

(15) Xia, X.; Zeng, J.; Oetjen, L. K.; Li, Q.; Xia, Y. Quantitative Analysis of the Role Played by Poly(vinylpyrrolidone) in Seed-Mediated Growth of Ag Nanocrystals. *Journal of the American Chemical Society*, 2012, *134*, 1793–1801.

(16) Wang, J.; Peng, H.-C.; Xia, Y.; Kim, M. J.; Lu, N.; Liu, M.; Xie, S.; Xia, X. On the role of surface diffusion in determining the shape or morphology of noble-metal nanocrystals. *Proceedings of the National Academy of Sciences*, 4AD, *110*, 6669–6673.

(17) Wickham, J.; Scher, E.; Peng, X.; Alivisatos, A. P.; Kadavanich, A.; Manna, L.; Yang, W. Shape control of CdSe nanocrystals. *Nature*, 2000, *404*.

(18) Xu, S.; Wang, A.; Jia, G. Emerging strategies for the synthesis of monodisperse colloidal semiconductor quantum rods. *Journal of Materials Chemistry C*, 2015, *3*, 8284–8293.

(19) Penn, R. L.; Ebert, T. T.; Zhang, H.; Welch, S. A.; Banfield, J. F. Aggregation-Based Crystal Growth and Microstructure Development in Natural Iron Oxyhydroxide Biomineralization Products. *Science*, 2000, *289*, 751–754.

(20) O'Sullivan, C.; Gunning, R. D.; Sanyal, A.; Barrett, C. A.; Geaney, H.; Laffir, F. R.; Ahmed, S.; Ryan, K. M. Spontaneous Room Temperature Elongation of CdS and Ag2S Nanorods via Oriented Attachment. *Journal of the American Chemical Society*, 2009, *131*,

12250–12257.

(21) Koh, W.; Bartnik, A. C.; Wise, F. W.; Murray, C. B. Synthesis of Monodisperse PbSe Nanorods: A Case for Oriented Attachment. *Journal of the American Chemical Society*, 2010, *132*, 3909–3913.

(22) Yu, J. H.; Joo, J.; Park, H. M.; Baik, S.-I.; Kim, Y. W.; Kim, S. C.; Hyeon, T. Synthesis of Quantum-Sized Cubic ZnS Nanorods by the Oriented Attachment Mechanism. *Journal of the American Chemical Society*, 2005, *127*, 5662–5670.

(23) Weller, H.; Kornowski, A.; Pacholski, C. Self-Assembly of ZnO: From Nanodots to Nanorods. *Angewandte Chemie International Edition*, 2002, *41*, 1188–1191.

(24) Wang, Q.; Du, Y.; Peng, L.; Zhang, Y.; Shen, S. Matchstick-Shaped Ag2S–ZnS Heteronanostructures Preserving both UV/Blue and Near-Infrared Photoluminescence. *Angewandte Chemie International Edition*, 2011, *50*, 7115–7118.

(25) Ouyang, L.; Maher, K. N.; Yu, C. L.; McCarty, J.; Park, H. Catalyst-Assisted Solution−Liquid−Solid Synthesis of CdS/CdSe Nanorod Heterostructures. *Journal of the American Chemical Society*, 2007, *129*, 133–138.

(26) Li, L.; Jahanian, P.; Mao, G. Electrocrystallization of Tetrathiafulvalene Charge-Transfer Salt Nanorods on Gold Nanoparticle Seeds. *The Journal of Physical Chemistry C*, 2014, *118*, 18771–18782.

(27) Keefer, K. D.; Washecheck, D. M.; Enright, N. P.; Williams, J. M. *J. Am. Chem. Soc.* **1976**, *98*, 233–234.

(28) The Morphology Prediction of Lysozyme Crystals Deduced from the BFDH Law and Attachment Energy Model Based on the Intermolecular Interaction - IEEE Xplore Document, 2017.

(29) Scharifker, B. R.; Borrás, C.; Díaz-Morales, O.; Mostany, J. Current transient study of the kinetics of nucleation and diffusion-controlled growth of bimetallic phases. *Journal of Solid State Electrochemistry*, *17*, 345–351.

(30) Radisic, A.; Vereecken, P. M.; Searson, P. C.; Ross, F. M. The morphology and nucleation kinetics of copper islands during electrodeposition. *Surface Science*, 2006, *600*, 1817–1826.

(31) Grujicic, D.; Pesic, B. Electrodeposition of copper: the nucleation mechanisms. *Electrochimica Acta*, 2002, *47*, 2901–2912.

(32) C. Loveday, D.; Robert Hillman, A.; Guy Orpen, A.; G. Pringle, P.; Maria Hepel. Electrochemical quartz crystal microbalance studies of partially oxidized tetracyanoplatinum salts. *Journal of Materials Chemistry*, 1996, *6*, 993–998.

(33) Fichthorn, K. A.; Qi, X.; Balankura, T. Multi-scale theory and simulation of shape-selective nanocrystal growth. *CrystEngComm*, 2016, *18*, 5410–5417.

(34) Fichthorn, K. A. Atomic-Scale Theory and Simulations for Colloidal Metal Nanocrystal Growth. *Journal of Chemical & Engineering Data*, 2014, *59*, 3113–3119.

(35) Balankura, T.; Qi, X.; Zhou, Y.; Fichthorn, K. A. *J. Chem. Phys.* **2016**, *145*.

(36) Hwang, N.-M.; Lee, D.-K.; Jung, J.-S. Thermodynamics and Kinetics in the Synthesis of Monodisperse Nanoparticles, 2012.

(37) Chong, W. H.; He, J.; Chen, H.; Liu, C.; Wang, Y. Thermodynamics versus Kinetics in Nanosynthesis. *Angewandte Chemie International Edition*, 2015, *54*, 2022–2051.

(38) Modeling crystal growth from solution with molecular dynamics simulations: Approaches to transition rate constants: The Journal of Chemical Physics: Vol 136, No 3, 2017.

(39) Kinetics modeling of nanoparticle growth on and evaporation off nanotubes:

Journal of Applied Physics: Vol 121, No 1, 2017.

(40) Shekhar, H. Thermodynamics of gold nanoparticle growth: A first-principles investigation, 2013.

(41) Chrzan, D. C.; Haller, E. E.; J. W. Ager, I. I. I.; Liao, C. Y.; Yi, D. O.; Jhon, M. H.; Sharp, I. D.; Xu, Q.; Yuan, C. W. Modeling nucleation and growth of encapsulated nanocrystals: Kinetic Monte Carlo simulations and rate theory. *Physical Review B*, 2008, *78*.

(42) Tang, Q.; Jiang, D.; Mirkin, C. A.; Personick, M. L.; Zhang, P.; Padmos, J. D.; Duchesne, P. N. The surface structure of silver-coated gold nanocrystals and its influence on shape control. *Nature Communications*, 2015, *6*.

(43) Wiley: Simulation and the Monte Carlo Method, Third Edition - Reuven Y. Rubinstein, Dirk P. Kroese, 2017.

(44) Harinipriya, S.; Subramanian, V. R. *J. Phys. Chem. B* **2008**, *112*, 4036–4047.

(45) Treeratanaphitak, T.; Pritzker, M. D.; Abukhdeir, N. M. *Electrochimica Acta* **2014**, *121*, 407–414.

(46) Pricer, T. J.; Kushner, M. J.; Alkire, R. C. *J. Electrochem. Soc.* **2002**, *149*.

(47) Guo, L.; Radisic, A.; Searson, P. C. *J. Phys. Chem. B* **2005**, *109*, 24008–24015.

ABSTRACT

ENGINEERING OF ORGANIC NANOCRYSTALS BY ELECTROCRYSTALLIZATION

by

MOHAMED KILANI

May 2017

Advisor: Dr. Guangzhao Mao
Major: Material Science & Engineering
Degree: Master of Science

This work discusses the experimental and theoretical methods used to control the morphology of nanocrystals. The hypothesis of the thermodynamic/kinetic control of the morphology was verified. We applied the electrocrystallization to make K*(def)*TCP nanocrystals and we tuned the electrochemical parameters to determine their influence on the nanocrystals morphologies. The characterization was mainly performed with AFM and FE-SEM. We presented in this work the possibility to control the morphology of K*(def)*TCP using the electrochemical parameters. The obtained shapes ranged from nanorods to rhombohedral shape, which is reported for the first time. The observed growth behavior was modeled and simulated with a method based on Monte-Carlo techniques. The simulation results show a qualitative match with the experimental findings. This work contributes to the understanding of the crystal growth behavior and the thermodynamic/kinetic morphology transition using electrocrystallization.

AUTOBIOGRAPHICAL STATEMENT

MOHAMED KILANI

EDUCATION:

M.S.	Wayne State University	Materials Science & Engineering	2017
M.S.	National engineering school of Sousse	Mechanics and systems engineering	2012
B.S.	National engineering school of Sousse	Mechatronics Engineering	2011

APPOINTMENTS:

8/2015 – Present	M.S. in Materials Science, Wayne State University
7/2011 – 6/2015	Project Manager, Genovia Ingenierie - Tunisia (FEA for the automotive industry)
9/2010 – 12/2012	M.S. in Mechanics and Systems Engineering, National engineering school of Sousse
9/2008 – 6/2011	B.S. in Mechatronics Engineering, National engineering school of Sousse
9/2006 – 6/2008	Preparatory Institute for engineering studies of Nabeul

HONORS AND AWARDS:

1. Fulbright Scholarship to pursue a Master at Wayne State University - 2015
2. Best Engineer of the company, Genovia Ingenierie - 2013
3. 1st Place – Mechanics and Systems engineering, Sousse, Tunisia – 2012
4. 1st Place – Mechatronics, Sousse, Tunisia – 2009
5. Best Student – Technological Section, Beja, Tunisia – 2006

PUBLICATIONS:

1. "Electrodeposition of Partially Oxidized Tetracyanoplatinate Nanowires on Seeds and Electrical Patterns for Gas Sensing" Jahanian P., Yu X., Kilani M., and Mao G. (submitted)
2. "Enhanced modeling of the induced compressibility by damage in natural polymers" Mohamed Kilani, Zoubeir Tourki – University of Sousse Library (2012)
3. "Design of fast loads machine for spot welded joints characterization" Mohamed Kilani, Hechmi Bendali – University of Sousse Library (2011)